

# Prediction of volume of shallow landslides due to rainfall using data-driven models

Tuganishuri Jérémie<sup>1</sup>, Chan-Young Yune<sup>2</sup>, Gihong Kim<sup>3</sup>, Seung Woo Lee<sup>4</sup>, Manik Das Adhikari<sup>5</sup>, and, Sang-Guk Yum<sup>6\*</sup>

<sup>1</sup>Department of Civil and Environmental Engineering, Gangneung-Wonju National University, Gangneung, Gangwon 25457, South Korea

<sup>2</sup>Department of Civil and Environmental Engineering, Gangneung-Wonju National University, Gangneung, Gangwon 25457, South Korea

<sup>3</sup>Department of Civil and Environmental Engineering, Gangneung-Wonju National University, Gangneung, Gangwon 25457, South Korea

<sup>4</sup>Department of Civil and Environmental Engineering, Gangneung-Wonju National University, Gangneung, Gangwon 25457, South Korea

<sup>5</sup>Department of Civil and Environmental Engineering, Gangneung-Wonju National University, Gangneung, Gangwon 25457, South Korea

<sup>6</sup>Department of Civil and Environmental Engineering, Gangneung-Wonju National University, Gangneung, Gangwon 25457, South Korea

Correspondence to: Sang-Guk Yum (skyeom0401@gwnu.ac.kr)

**Abstract.** Landslides due to rainfall are among the most destructive natural disasters that cause property damages, huge financial losses, and human deaths in different parts of the World. To plan for mitigation and resilience, the prediction of the volume of rainfall-induced landslides is essential to understand the relationship between the volume of soil materials debris and their associated predictors. The objectives of this research are to construct a model using advanced data-driven algorithms (i.e., ordinary least squares or Linear regression (OLS), random forest (RF), support vector machine (SVM), extreme gradient boosting (EGB), generalized linear model (GLM), decision tree (DT), deep neural network (DNN),  $k$ -nearest neighbor (KNN) and Ridge regression (RR)) for the prediction of the volume of landslides due to rainfall, considering geological, geomorphological, and environmental conditions. Models were trained and tested on South Korean landslide dataset, with the EGB predictions yielding the highest coefficient of determination ( $R^2 = 0.8841$ ) and the lowest mean absolute error ( $MAE = 146.6120 \text{ m}^3$ ), followed by RF predictions ( $R^2 = 0.8435$ ,  $MAE = 330.4876 \text{ m}^3$ ) on the holdout set. The results indicated that the DNN, EGB, and RF models exhibited  $R^2 > 0.8$  on both the training and test sets. The difference in coefficient of determination  $R^2$  on the training and holdout set were 1.75, 7.72, and 12.17% for RF, EGB and DNN, respectively, signifying that these models could yield reliable volume estimates in adjacent areas with similar geomorphological and environmental settings. The volume of landslides was strongly influenced by slope length, maximum hourly rainfall, slope angle, aspect, and altitude. The anticipated volume of landslides can be important for land use allocation and efficient landslide risk

37 management.

38

39 **Keywords:** Data-driven models, shallow landslides, predictive machine learning, Rainfall-Induced Slope Failure,  
40 Landslides Volume Prediction, South Korea

41

## 42 **1. Introduction**

43 Landslides due to rainfall are phenomena that dislocate a mass of soil from its natural position and slide downward  
44 along a slope due to gravity forces. Intense or long-duration rainfall infiltrates the soil and increases the pore pressure,  
45 resulting in soil saturation that leads to slope failure. The saturated soil becomes weak and loses cohesion, and the  
46 slope fails when rainfall crosses a certain threshold (Bernardie et al., 2014; Martinović et al., 2018; Lee et al., 2021).  
47 The heavy rainfall saturates a slope and triggers a landslide due to the reduction of the soil's shear strength and the  
48 increase of pore water pressure (Tsai and Chen, 2010; Lacerda et al., 2014; Chatra et al., 2019; Chen et al., 2021;  
49 Luino et al., 2022). For example, steep slopes with loose soils and even moderate rainfall can lead to the displacement  
50 of an enormous quantity of soil mass. On the contrary, in slopes with more stable, cohesive soils, the surface failure  
51 might be smaller (Tsai and Chen, 2010). The rainfall quantity and duration influence the volume of the landslides; the  
52 higher the intensity and the longer the duration of rainfall, the larger the resulting surface failure (Chang and Chiang,  
53 2009; Bernardie et al., 2014; Chen et al., 2017). The landslide occurrences can also be influenced by human activities  
54 that weaken the slope, such as excavation at the slope toe and loading caused by construction and land use such as  
55 agriculture, mining etc. (Rosi et al., 2016). The rapid urbanization activities in mountainous regions affect the  
56 topography through hill cutting, deforestation and water drainage (Rahman et al., 2017); these activities disturb the  
57 slope structure and change the water flow, which exacerbates the effect of landslides in regions where human  
58 engineering activities are mostly located (Holcombe et al., 2016; Chen et al., 2019). Therefore, to mitigate landslide-  
59 induced risks in the runout regions, estimation of the volume of landslides due to rainfall (VLDR) plays a crucial role.

60 The quantification of the VLDR is essential for effective risk management (Tacconi Stefanelli et al., 2020),  
61 emergency response, engineering design (Cheung, 2021), economic assessment and environmental protection  
62 (Alcántara-Ayala and Sassa, 2023). With the estimates of VLDR, the morphologist can update hazard maps (Van  
63 Westen, 2000) to reflect the scale of potential mass movement in various regions to obtain regions with similar  
64 likelihood of landslides of similar soil mass to highlight risk zone levels, i.e., low, moderate and high. These  
65 classifications help engineers to apply appropriate slope stabilization techniques depending on the level of risk (Dahal  
66 and Dahal, 2017). Additionally, enhancing the precision of VLDR estimations and improving the predictive  
67 capabilities is essential for understanding and monitoring landscape evolution. Montgomery (2009) emphasized that  
68 the volume of landslides is a key factor in determining the extent of downstream damage, particularly for large debris  
69 flows or rock avalanches, which can drastically alter the landscape and affect surrounding ecosystems and  
70 infrastructure. Similarly, Korup (2004) further explored the long-term geomorphological effects of large-volume  
71 landslides, highlighting their importance in reshaping mountainous terrains and influencing sediment transport, which  
72 is critical for understanding both immediate and future landscape changes. However, the existing landslide

73 susceptibility models mostly used for the identification of regions susceptible to landslides (i.e., landslide zonation)  
74 (Kim et al., 2014; Gutierrez-Martin, 2020; Chen et al., 2021; Li et al., 2022), which are essential in emergency  
75 management because they provide a general overview of zones with a higher probability of landslide occurrence  
76 without emphasizing on the determination of the approximate value of the volume of failing mass in relation to  
77 excessive rainfall events.

78 Numerous researchers used landslide inventory, remote sensing data and numerical techniques to establish  
79 the relationship between landslide geometry and the influencing factors to determine the landslide volume  
80 quantitatively. For example, Saito et al. (2014) studied the relationship between rainfall-triggered landslides to test  
81 whether the volume of landslides across Japan that occurred between 2001 and 2011 can be directly predicted from  
82 rainfall metrics. The findings revealed that larger landslides occurred when rainfall exceeded certain thresholds, but  
83 there were significant discrepancies between peaks of rainfall metrics and maximum landslide volumes, and the total  
84 rainfall was the suitable predictor of landslides. Dai and Lee (2001) established the frequency-volume relation for  
85 landslides in Hong Kong and noticed that the relation for shallow landslides above 4m<sup>3</sup> followed the power law. The  
86 12-hour rolling rainfall contributed most to the prediction of the volume of landslides. Jaboyedoff et al. (2012)  
87 contributed by demonstrating the value of remote sensing technologies such as Light Detection and Ranging (LiDAR)  
88 in conjunction with field data to improve the accuracy of volume estimates and capture the geomorphological changes  
89 associated with landslides. Ju et al. (2023) constructed an area-volume power law model for the estimation of the  
90 volume of landslides using high-resolution LiDAR data collected between 2010 and 2020 in Hong Kong. The aim  
91 was to estimate accurately the volume of landslides on small-scale landslides. The reliance on localized datasets limits  
92 the model's applicability in regions with different geological settings, and the model does not consider all variabilities  
93 of landslide characteristics. Razakova et al. (2020) calculated landslide volume using remote sensing data to assess  
94 the efficiency of aerial photographs in environmental impact assessment and ground-based measurement. The study  
95 did not consider the effect of vegetation and topography and only focused on a single landslide case, which may be a  
96 source of bias due to differences in soil composition and environmental factors. Hovius et al. (1997) analyzed multiple  
97 sets of aerial photos and frequency-magnitude relations for landslides in New Zealand. The finding pinpointed that  
98 the landslides frequency-magnitude followed power law and infrequent large magnitude contributed to the landscape  
99 change. The study highlighted the importance of soil composition in landslide size, but the reliance on aerial photos,  
100 which may be inaccurate in dense forest areas, and the omission of climatic factors limit the generality of the findings.  
101 Guzzetti et al. (2008) applied statistical methods on regional landslide inventories and antecedent rainfall data ranging  
102 between 10 min to 35 days. The findings revealed that the slope angle and soil type significantly influence landslide  
103 volume estimates, and the rainfall intensity is more important than duration. Chatra et al. (2019) applied numerical  
104 methods to study the effect of rainfall duration and intensity on the generation of pore pressure in the soil; the finding  
105 revealed a higher instability in loose soil compared to medium soil slopes. Huang et al. (2020) introduced a hybrid  
106 machine-learning model combining support vector regression (SVR) with a genetic algorithm to estimate debris-flow  
107 volumes. The model was tested on real-world case studies, showing improved accuracy in volume predictions  
108 compared to traditional methods. However, it was noticed that the study relied on a limited dataset, which may reduce  
109 the model's generalizability to other regions of different geomorphology and environmental settings. Shirzadi et al.

110 (2017) compared the effectiveness of statistical and machine-learning models in simulating landslide volumes-areal  
111 relations, demonstrating that machine-learning techniques outperform traditional statistical methods in terms of  
112 accuracy. The study did not consider the climatic and geomorphic factors such as rainfall, vegetation, soil type, etc.,  
113 triggering and influencing factors for the landslide occurrence. It was noted that existing models only treated the  
114 interaction of soil and rainfall without considering the environmental factors, human activity, and non-linear behavior  
115 of the triggering and influencing factors.

116 In the present study, the volume of landslides due to rainfall is predicted using OLS, RF, SVM, EGB, GLM,  
117 DT, DNN, KNN and RR algorithms, considering the details of triggering factors (i.e., rainfall) and predisposing factors  
118 (i.e., geomorphological, soil and environmental). Here, we aim to construct a data-driven algorithm that combines  
119 input parameters for physical-based and empirical models and incorporates more complex non-linear features of input  
120 variables to predict the occurrence of associated events more accurately. The main assumption behind the data-driven  
121 algorithm is that the considered feature input of the model produces a similar volume of landslides due to rainfall and  
122 follows the same pattern at a particular region with the same features under the same quantity of rainfall. Here, we  
123 examine different machine learning (ML) algorithms and compare their performance using the coefficient of  
124 determinations ( $R^2$ ), mean square errors (MAE), Root mean square error (RMSE), Mean absolute percentage error  
125 (MAPE), and symmetric mean absolute percentage errors (SMAPE) of the predicted volume of landslides. The focus  
126 is to optimize the predictions of the volume of landslides due to rainfall, taking into account triggering and influencing  
127 factors with higher accuracy.

128

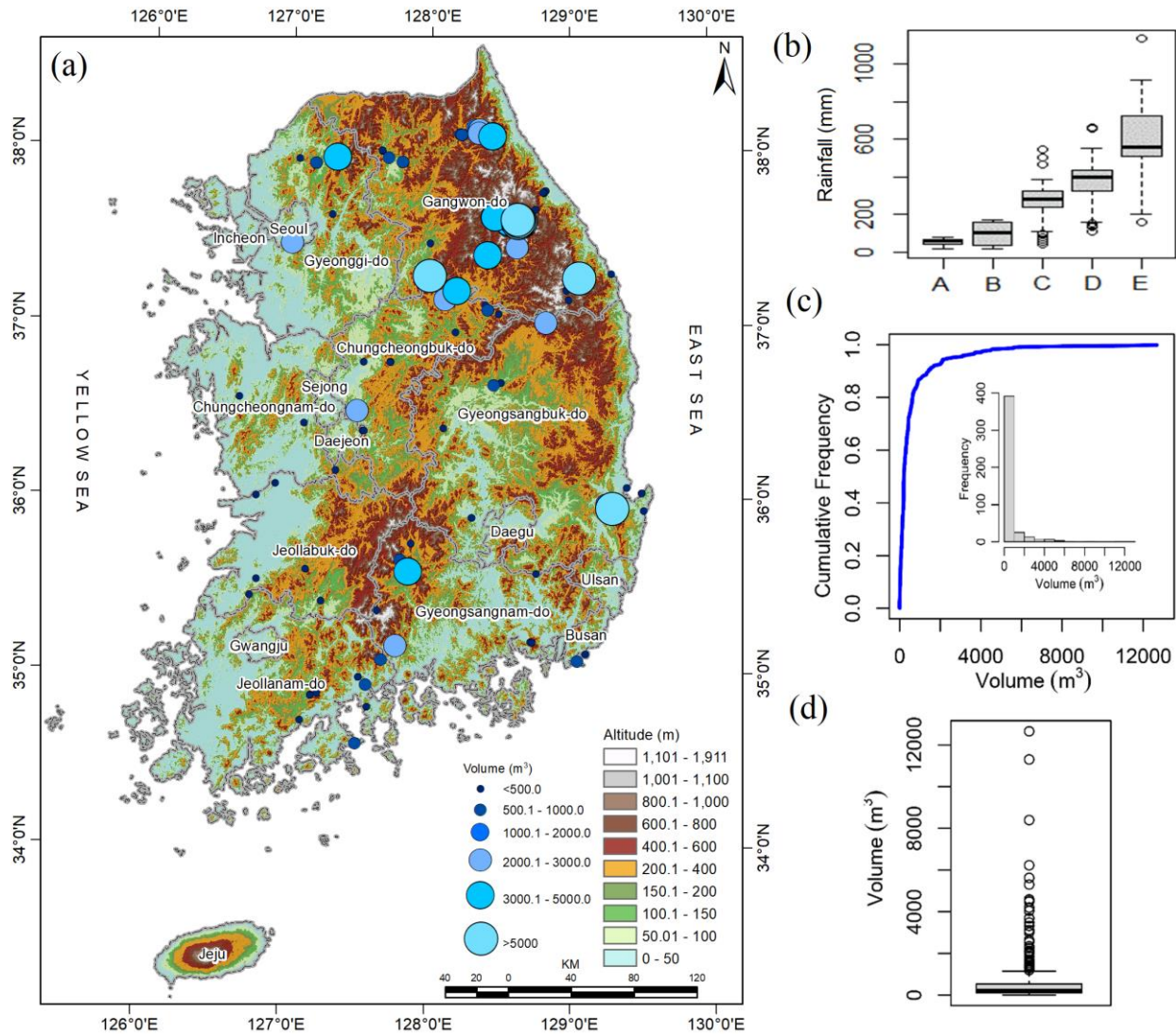
## 129 **2. Data and Study Region**

### 130 **2.1. Study Region**

131 The region for testing the model is South Korea, characterized by mountainous (63% of total land) relief, especially  
132 in the eastern part of the country (Lee et al., 2022). South Korea is located on the southern part of the Korean Peninsula,  
133 bordered by the Yellow Sea to the west coast and the East Sea (Sea of Japan) to the East. According to the Korean  
134 Meteorological Administration (<https://www.kma.go.kr/>), the country has a temperate climate characterized by four  
135 distinct seasons: hot and humid summers, cold winters, and springs and falls with moderate temperatures. The annual  
136 rainfall varies between 1000 mm to 1400 mm and 1800 mm for the central region and southern region, respectively  
137 (Jung et al., 2017; Alcantara and Ahn, 2020). During the summer, heavy rainfall from June to September leads to  
138 significant surface runoff, increases landslide risk, and causes approximately 95% of all landslides each year (Lee et  
139 al., 2020; Park and Lee, 2021). In addition, the landslides may be aggravated by typhoons, which mostly occur in  
140 August and September, and it is anticipated that frequency will increase due to climate change (Kim and Park, 2021).  
141 The rainfall trend analysis from 1971 to 2100 predicted an increase in rainfall of 271.23mm, which indicates the  
142 growing risk of landslides associated with climate change (Lee, 2016). Temperature variations are influenced by its  
143 geographical location; the average summer temperatures vary between 25 and 30°C, while winter temperatures can  
144 drop to -10°C in some parts of the country (<https://web.kma.go.kr/>). The South Korean geologically is mainly  
145 composed of granitic and metamorphic rocks, such as gneiss, schist, and granite, which influence the stability of the  
146 landscape (Jung et al., 2024). The geomorphology is characterized by rugged mountains, river valleys, and coastal

147 plains, with the Taebaek Mountains running along the eastern edge (Kim et al., 2020). The influence of rainfall,  
148 environmental, geomorphology, and geological factors increase the vulnerability to landslides across the country,  
149 especially in the northeastern mountainous region, as depicted in Figure 1. The predominant soil types in South Korea  
150 include clay, sandy, and loamy soils, each with different characteristics affecting water infiltration, retention and  
151 erosion (Kang et al., 2022; Lee et al., 2023). Clay soils, being more stable, can become highly saturated, increasing  
152 landslide risk during heavy rains. On the other hand, sandy soils are loose and more prone to shallow landslides during  
153 light rainfall. Regions with steep topography and poorly consolidated soil (loose) are mostly at risk, especially after  
154 prolonged rainfalls (Kim et al., 2015).

155         The combination of heavy summer rainfall, geological composition, and geomorphological factors makes  
156 South Korea particularly vulnerable to shallow landslides. Thus, continuous monitoring and research are vital to  
157 understanding the complex interactions between climate, geology, soil types, and landslide occurrences in this region.  
158 Understanding the collective effects of meteorological, environmental, geological stability, and geomorphological  
159 features is crucial for developing effective disaster management strategies and enhancing public safety in landslide-  
160 prone areas. As climate change continues to impact rainfall patterns, South Korea faces ongoing challenges in  
161 mitigating landslide risks and protecting vulnerable communities.



162  
 163 **Figure 1: (a) Spatial distribution of landslides in South Korea, (b) Temporal variation of rainfall, i.e., A: Maximum hourly**  
 164 **rainfall, B: Four weeks rainfall, C: Three hours rainfall, D: Three days rainfall and E: Two weeks rainfall, (c)**  
 165 **Cumulative frequency distribution of the volume of landslides, and (d) Box plot of the volume of landslides.**  
 166 **(The elevation data presented in Fig. 1a is sourced SRTM DEM, downloaded from**  
 167 **<https://earthexplorer.usgs.gov/>).**

168  
 169 **2.2 Data**

170 The landslide inventory dataset contains 455 landslide record information from 2011 to 2012, collected from different  
 171 locations in South Korea through field survey, and the vegetation and forest fire features were obtained from Korean  
 172 Forest Services database. The combined dataset tabulates information on landslide geometry, such as runout length,  
 173 width, depth, and volume of the affected area, along with geomorphological composition, vegetation, and antecedent  
 174 rainfall prior to landslide events. The details regarding landslide predisposing and triggering factors are summarized  
 175 in Table 1.

176 The majority of landslides in this region were shallow, translational slope failures (Kim et al., 2001). The  
 177 occurred landslides had a volume varying between 1.5m<sup>3</sup> to 12,663m<sup>3</sup> and predominantly occurred in the northeastern  
 178 and southeastern region (Figs. 1a,c-d). The landslides that occurred exhibited a hollowed morphology and a rightward  
 179 skew in the distribution of their volumes with 2570.7m<sup>3</sup> as 95<sup>th</sup> quantile, with the largest volume 12,663m<sup>3</sup>, and the  
 180 aggregate mass of landslide due to rainfall was 276,986.62m<sup>3</sup>. The estimation of the volume of removed material by  
 181 landslides is important as it helps to assess risks the estimated damage can cause down at the toe of the failed slope,  
 182 such as blocking transportation network, burying crops or farmland, the damage-built environment near landslide risks  
 183 area, and post-disaster recovery planning (Evans et al., 2006; Rotaru et al., 2007; Intrieri et al., 2019).

184

185 **Table 1: Landslide influencing and triggering factors.**

Group	Features	Feature Relevance	References
Vegetation	Fire history	The burning of the vegetation intensifies the mass movement of soil near the uncovered burned stem of trees and free movement on uncovered soil due to post-fire rainfall and storms. The sliding may also be due to loss of vegetation, altered soil property and structure. These lead to soil degradation and higher infiltration, which increase the pore pressure, and change in hydrology by concentrating water flow in places that exacerbate landslides.	Highland and Bobrowsky, 2008; Stoof et al., 2012; Hyde et al., 2016; Culler et al., 2021
	Age of tree	Mature forests have more resistance to shallow landslides due to highly developed roots, which improve soil cohesion and leaves that prevent direct contact of raindrops with the soil surface.	Sato et al., 2023; Lann et al., 2024
	Forest density	The presence of forest reduces the likelihood of landslides about three times compared to grassland. Grassland has been revealed to be three times more vulnerable to shallow landslides than broadleaf, coniferous, and secondary forests.	Greenwood et al., 2004; Turner et al., 2010; Scheidl et al., 2020; Asada and Minagawa, 2023; Lann et al., 2024
	Timber diameter (m)	Tree spacing and size were used to investigate the effect of root and tree in shallow landslide control. High root density generally enhances slope stability, and specific tree placement and root sizes between 5 to 20 mm effectively prevent landslides.	Wang et al., 2016; Cohen and Schwarz, 2017
Geomorphology	Drainage	The drainage significantly affects slope stability and promotes efficient control of rainfall's influence on groundwater fluctuation. The presence of drainage increases the threshold of landslides due to rainfall.	Korup et al., 2007; Sun et al., 2010; Yan et al., 2019; Wei et al., 2019
	Slope angle (°)	The steeper slopes have a lower presence of landslides due to the low transportable materials. Slopes between 20-40 degrees are most vulnerable to greater landslides as rainfall intensity and duration increase. Generally, the average angle of the terrain at the landslide location provides valuable insight into the region's overall	Donnarumma et al., 2013; Duc, 2013; Qiu et al., 2016

Group	Features	Feature Relevance	References
		steepness and geomorphic characteristics, which are crucial factors for landslide susceptibility and risk modeling.	
	Slope aspect	The effect of rainfall on slope differs by slope angle and slope aspect, which leads to unevenly distributed landslides.	Panday and Dong, 2021; Celtek, 2021
	Slope length (m)	The volume increases as the slope length increases. A complex interplay exists between rainfall, length of slope and slope angle in the occurrence of landslides.	Turner et al., 2010
	Soil depth (m)	Soil properties, depth, and texture have significant differences in infiltration rates, which have different influences on the occurrence of landslides.	Kitutu et al., 2009; McKenna et al., 2012
	Soil type	Soil types, namely, Sandy loam, silt loam and loam, with their coefficient of permeability 1.7, 1.65 and 1.5, respectively, retain water differently, leading to different saturation times. The soil with higher permeability tends to drain water more efficiently, making it less prone to saturation. In contrast, the soil with lower permeability, the pore pressure may rapidly increase leading to shallow landslide initiation during intense rainfall events.	Chen et al., 2015; Liu et al., 2021a
Location	Altitude	Regional variability of elevation and mountain steepness affect the quantity of rainfall and associated landslides.	Um et al., 2010; Hyun et al., 2010; Yoon and Bae, 2013; Park, 2015
	Maximum hourly rainfall	The rainfall infiltrates the slope and increases pore water pressure, which reduces soil shear strength and leads to soil saturation, that causes surface failure.	Wieczorek, 1987; Dai and Lee, 2001; Smith et al., 2023
Rainfall	Continuous rainfall	Sudden intense rainfall concentrated in short periods is responsible for shallow landslides and debris flow.	Zhang et al., 2019
	Three hours rainfall		
	Three days rainfall	The antecedent rainfalls increase moisture in the soil and weaken soil cohesion.	Bernardie et al., 2014; Chen et al., 2015; Gariano et al., 2017; Zhang et al., 2019; Ran et al., 2022
	Two weeks rainfall		
	Four weeks rainfall		

186

187

188

189

190

191

192

193

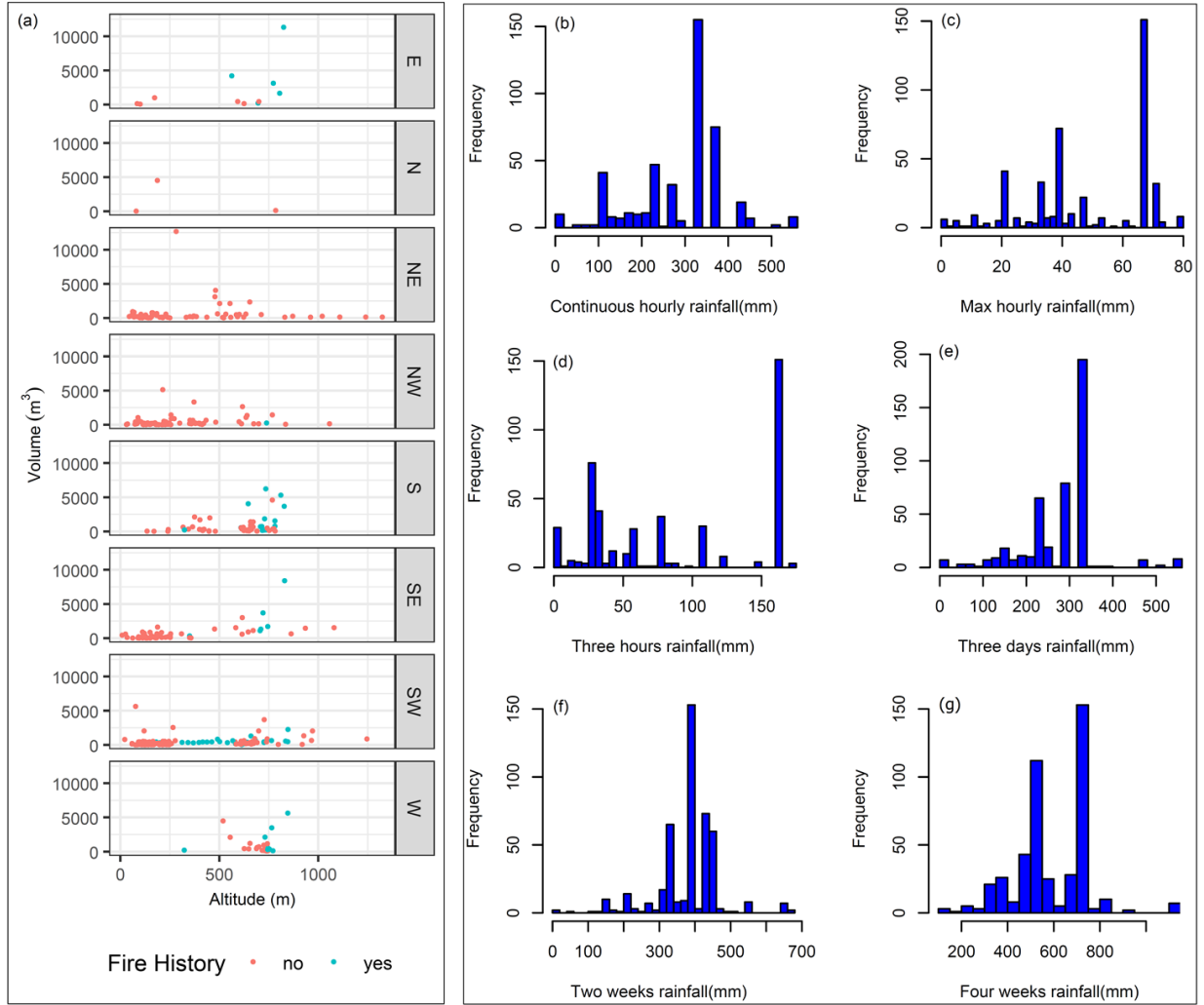
194

Location parameters such as altitude, latitude and longitude are essential elements that determine the microclimate of a given region, influencing rainfall patterns (Hyun et al., 2010; Yoon and Bae, 2013; Park, 2015). The northeastern region is characterized by high-elevation terrain, such as the Taebaek and Sobaek ranges, which dry air and lead to orographic precipitation (Yun et al., 2009). The windward mountain versants receive a substantial amount of rainfall, which can increase the likelihood of landslides (Jin et al., 2022). This variation of rainfall with respect to the direction highlights the importance of including slope aspect variables in landslide studies (Kunz and Kottmeier, 2006). Figure 2(a) depicts the relationship between the slope aspect and the volume of landslides and slope aspect, altitude and fire history and shows that larger volumes were localized in regions that faced forest fire and altitudes



195 between 500 and 1000m. Additionally, the topographical features such as slope length and slope angle affect the size  
196 of the landslide (Panday and Dong, 2021), slope failure due to over-saturation from groundwater and rainfall  
197 infiltration that destabilize the slope (Kafle et al., 2022). Furthermore, slope length, slope angle and slope aspect play  
198 an important role in the determination of the volume of geological material uprooted by landslides (Zaruba and Mencl,  
199 2014; Khan et al., 2021). The slope stability depends on soil composition properties, including soil permeability  
200 indices that affect water infiltration and saturation level (Chen et al., 2015). In the study regions, three main soil types,  
201 namely, sandy loam, loam, and silt loam, were observed, and their coefficient of permeability is 1.7, 1.65 and 1.5,  
202 respectively (Lee et al., 2013). Moreover, to reduce infiltration, the drainage network channels rainwater, drains the  
203 soil, and reduces saturation, which minimizes the likelihood of landslide occurrence due to groundwater discharge and  
204 surface runoff (Hovius et al., 1997; Wei et al., 2019). Furthermore, the vegetation protects the topsoil from the direct  
205 impact of raindrops hitting the ground, which causes erosion due to the force of gravity and reduces infiltration  
206 (Omwega, 1989; Keefer, 2000). The absence of vegetation allows rainwater to seep away fine topsoil, causing shallow  
207 landslides (Gonzalez-Ollauri and Mickovski, 2017). On the contrary, vegetation improves soil cohesion and prevents  
208 potential shallow landslides due to soil-root interaction (Gong et al., 2021; Phillips et al., 2021). The density of  
209 vegetation (forest) and leafage type (broad, pines or mixture) directly affects the quantity of raindrops intercepted and  
210 prevented from directly hitting the soil, which emphasizes the contributions of vegetation in the landslides mitigation.  
211 Further, the occurrence of forest fires can contribute to the occurrence of landslides due to the burning of vegetation  
212 covering the area, changing soil properties and increasing soil pH (Lee et al., 2013).

213 The rainfall, a triggering factor of landslides, is the immediate cause of slope instability and failure due to  
214 infiltration that leads to saturation resulting from increased pore water pressure that reduces soil shear strength (Yune  
215 et al., 2010; Khan et al., 2012; Kim et al., 2021; Lee et al., 2021). The antecedent rainfall increases the moisture in the  
216 soil, which accelerates the soil saturation; the cumulative effect is essential to understand the saturation levels (Ran et  
217 al., 2022). In this study, rainfall variables are grouped based on time, namely, continuous rainfall, which is the  
218 accumulative value of rainfall on the day of a landslide from rainfall start hour to the landslide event, maximum hourly  
219 rainfall, rainfall during the fixed period such as three hours, one day, three days, two weeks etc. (Fig. 1b). The  
220 histograms for rainfall considered in this study are depicted in Figure 2(b-g). The descriptive statistics for all  
221 continuous variables are illustrated in Table 2.



222  
 223 **Figure 2: (a) The scatter plot showing the variation of landslide volumes with respect to slope aspect, fire history and**  
 224 **altitude, and (b-g) Histograms of rainfall distribution.**

225  
 226 **Table 2: Summary statistics for continuous variables.**

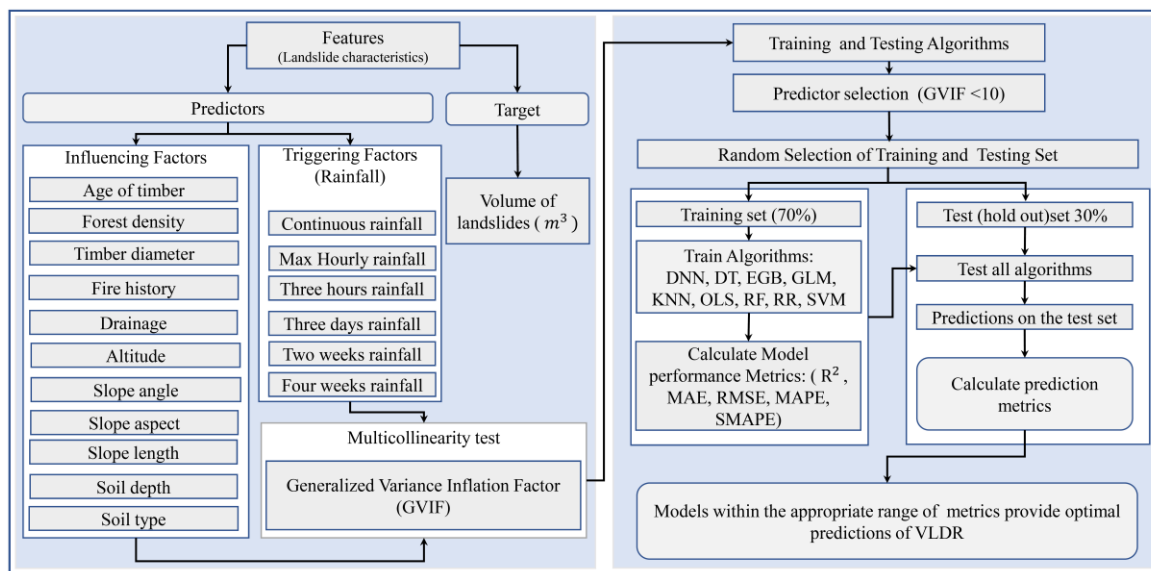
Variables	Units	N	Min	Mean	Median	Max	Std dev
Max Hourly rain	mm	455	0	48	48	78	20
Continuous rainfall	mm	455	0	285	327	550	106
Three hours rainfall	mm	455	0	88	80	171	60
Twelve Hours rainfall	mm	455	0	150	99	447	95
One day rainfall	mm	455	0	202	162	538	112
Three days rain	mm	455	0	280	284	550	86
Seven days rain	mm	455	0.5	323	330	634	88
Two weeks rain	mm	455	0.5	385	400	663	90
Three weeks rain	mm	455	86	504	533	914	115

Variables	Units	N	Min	Mean	Median	Max	Std dev
Four weeks rain	mm	455	108	587	561	1135	160
Soil depth	m	455	0.2	0.6	0.75	0.75	0.19
Soil type	-	455	1.5	1.6	1.5	1.7	0.087
Timber diameter	m	455	0.15	0.27	0.23	0.35	0.086
Age of tree	Years	455	10	34	35	60	14
Slope length	m	455	1.8	21	13	180	23
Slope angle	Degree (°)	455	10	34	34	65	7.9
Altitude	m	455	9	391	272	1324	273

227

### 228 3. Methods

229 In this paper, we consider nine data-driven models, namely OLS, RF, SVM, EGB, GLM, DT, DNN, KNN and RR, to  
 230 predict the volume of landslides due to rainfall. The model is tested on the South Korean landslides inventories and  
 231 predisposing factors coupled with triggering factors, i.e., rainfall data. The detailed workflow is summarized in Figure  
 232 3. The steps for construction of these models can be briefly summarized as follows: a) the dataset for landslide  
 233 inventories is cleaned and combined with rainfall dataset, b) the collinearity analysis is performed using variance  
 234 inflation factor, c) continuous feature are scaled (Z-score) (Bonamutial and Prasetyo, 2023) to facilitate algorithms to  
 235 converge fast, d) the dataset is split into training and test set, e) all models are tested on the same training set, and the  
 236 model evaluation on the test set using mean absolute error (MAE), coefficient of determination ( $R^2$ ), root mean square  
 237 error (RMSE), symmetric mean absolute percentage error (SMAPE) and mean absolute percentage error (MAPE) for  
 238 the comparison of actual and predicted volume by each model, f) variable importance is calculated for the optimal  
 239 model, and g) the distance correlation is calculated for each continuous feature, and Kruskal-Wallis and Dunn test are  
 240 conducted to examine the similarity of the effect of each category on the landslide volume.



241

242 **Figure 3: Workflow for the prediction of the volume of landslides due to rainfall.**

243

### 244 **3.1 Model Construction**

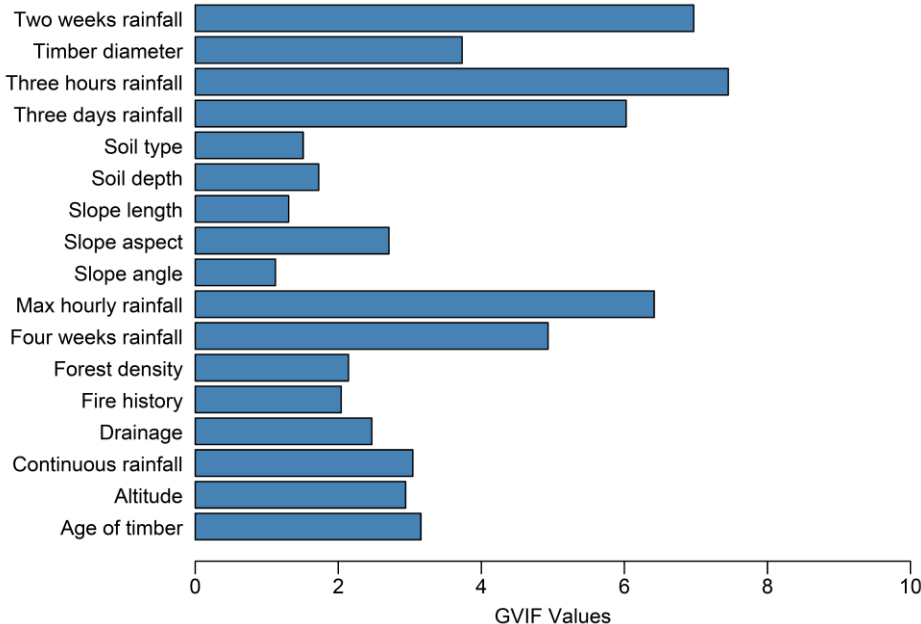
245 In the present investigation, we aimed to predict landslide volume using models that minimize error with  
246 interpretability and scalability. Since one model can not have all properties simultaneously, we selected some widely  
247 used models due to their inherent interpretability and scalability properties. The OLS, GLM, and DT were widely used  
248 for their high interpretability, which helps to understand the influence of individual features on predictions (Gelman  
249 and Hill, 2007; Breiman, 2017). On the other hand, the EGB, RF, SVM, RR, and KNN were used due to their robust  
250 performance in capturing complex patterns in data, which is essential for accurate predictions of landslide volumes  
251 (Liaw and Wiener, 2002; Hastie, 2009; Chen et al., 2022). Additionally, considering that the model will be used on a  
252 regional scale, which will require big data, the EGB, RF, and DNN are designed to efficiently handle large datasets,  
253 making them suitable for the regional scale analysis. These last models can be scaled to incorporate more data from  
254 different geographical areas without significant adjustments, enhancing their applicability in future research  
255 (Krizhevsky et al., 2012). Accordingly, nine data-driven methods were selected and tested on a Korean dataset to  
256 predict VLDR.

257 The first considered method is OLS, which is applied to estimate parameters of multilinear regression that  
258 yield the minimum residual sum of squares errors from the data (Kotsakis, 2023) under assumptions of no correlation  
259 in independent variables and error term, constant variance in error terms, non-linear collinearity of predictors, and  
260 normal distribution of error terms. The RF-regression is a supervised data-driven technique based on ensemble  
261 learning, which constructs many decision trees during the training time of a model by combining multiple decision  
262 trees to produce an improved overall result of the model outcome. The RF-regression is more efficient in the analysis  
263 of multidimensional datasets (Borup et al., 2023). RF is an effective predictive model due to non-overfitting  
264 characteristics based on the law of large numbers (Breiman, 2001). The DT regression is a predictive modeling  
265 technique in the form of a flowchart-like tree structure that includes all possible results, output, predictor costs, and  
266 utility. The DT simplifies the decision-making due to its algorithm that mimics human brain decision-making patterns  
267 (Rathore and Kumar, 2016). The KNN technique draws an imaginary boundary in which prediction outcomes are  
268 allocated as the average of  $k$ -nearest point predictors and averaging their output variable (response). The KNN  
269 calculates Euclidian distances to identify the likeness between datapoints, and then it groups points that have smaller  
270 distances between them (Kramer and Kramer, 2013). The RR is an improved form of ordinary least squares, which  
271 serves to respond to cases where collinearity is found in predictor variables. The estimated coefficients of ridge are  
272 biased estimators of true coefficients and are generated after adding a penalty on the OLS model. The RR has always  
273 lower variances compared to OLS (Saleh et al., 2019). The advantage of the GLM over OLS is that the dependent  
274 variable need not follow the normal distribution. The GLM is composed by random and systematic components and  
275 the link function that links the two. In this study, the GLM with Gaussian link function was applied. GLM is fitted  
276 using maximum likelihood estimation (Dobson and Barnett, 2018). The DNN is among data-driven models that  
277 revolutionized different fields; the DNN learns via multi-processing layers and identifies intricate patterns in the data  
278 to predict the outcome (LeCun et al., 2015). Here, the backpropagation algorithm was used to predict the estimated  
279 outcome. The advantage of DNN is that it can discover the complex structures in the data using a back propagation

280 algorithm capable of changing the internal parameter (weight update). The SVM is popular for balanced predictive  
 281 performance which makes it capable to train model on small sample size (Pisner and Schnyer, 2020). Subsequently,  
 282 SVM has been applied in many different landslide studies (Pham et al., 2018; Miao et al., 2018). SVM methods  
 283 identify the optimal hyperplane in multidimensional space that separates different groups in the output values. The  
 284 EGB is the most powerful and leading supervised machine learning method in solving regression problems. It can  
 285 perform parallel processing on Windows and Linux (Chen et al., 2022). The gradient boosting trains of differentiable  
 286 loss function, and the model fits when the gradient is minimized. In this paper, both traditional statistical predictive  
 287 models and ML models were used. The firsts are known for high clarity and explainability, and the second is famous  
 288 for handling non-linearity in features. In some cases, the performance of advanced data-driven algorithms is almost  
 289 similar (Chowdhury et al., 2023).

290  
 291 **3.2 Feature Selection and Data Splitting**

292 The variable selection procedure was based on previous literature and applied in the model using generalized  
 293 variance inflation factor (GVIF) (O’Brien, 2007) to eliminate collinear variables. The variable with  $GVIF < 10$  was  
 294 considered non-collinear and used in the model. Figure 4 depicts retained features and corresponding GVIF values.  
 295 The retained features have GVIF less than 10 (O’Brien, 2007). Accordingly, all depicted variables were considered for  
 296 the model training. Further, to train the model, the datasets were split randomly, with 70% of the data for the training  
 297 set and 30% for testing (Nguyen et al., 2021). The 10-fold cross-validation was performed to obtain an optimal model.  
 298 The training and test set was scaled (Z-score or variance stability scaling) to solve convergence issues that are  
 299 associated with running the model without feature scaling (Singh and Singh, 2022). To run the model on the data using  
 300 driven methods that accept numerical features only, the test and training set was one-hot-encoded to create a feature  
 301 matrix (Seger, 2018).  
 302



303  
 304 **Figure 4: Generalized Variance Inflation Factor (GVIF) bar plot for features.**

305 **3.3 Model Evaluation Metrics**

306 The model performance evaluation is a process of quantifying the difference between the observed value not  
 307 used in the modeling process and the predicted value by the model. Different metrics are applied depending on the  
 308 type of task, whether it is a classification or a regression problem. Subsequently, the widely used evaluation metrics  
 309 for regression models, namely,  $R^2$ , MAE, RMSE, MAPE and SMAPE, were utilized to evaluate the model  
 310 performances. The metric formulae and evaluation criteria are summarized in Table 3.

311

312 **Table 3: Model evaluation metrics.**

Metrics	Evaluation	References
$RMSE = \sqrt{\frac{1}{n} \sum_{i=1}^n (y_i - \hat{y}_i)^2}$	<ul style="list-style-type: none"> <li>Measures the square root of the average squared differences between predicted and actual values.</li> <li>Lower values indicate better model performance.</li> </ul>	Hyndman and Koehler, 2006
$MAE = \frac{1}{n} \sum_{i=1}^n  y_i - \hat{y}_i $	<ul style="list-style-type: none"> <li>The average of the absolute differences between predicted and actual values.</li> <li>Lower values indicate better model performance.</li> </ul>	Willmott and Matsuura, 2005
$MAPE = \frac{100}{n} \sum_{i=1}^n \left  \frac{y_i - \hat{y}_i}{y_i} \right $	<ul style="list-style-type: none"> <li>Measures the accuracy of a model as a percentage, which can be more interpretable.</li> <li>Lower values indicate better model performance.</li> </ul>	Armstrong, 2001
$SMAPE = \frac{100}{n} \sum_{i=1}^n \frac{ y_i - \hat{y}_i }{ y_i  +  \hat{y}_i }$	<ul style="list-style-type: none"> <li>Unlike MAPE, which can be skewed by very small actual values, SMAPE accounts for both the actual and predicted values, making it symmetric.</li> <li>SMAPE is expressed as a percentage</li> <li>Mitigates the impact of small actual values on the error metric, providing a more balanced assessment.</li> <li>Lower values indicate better model performance.</li> </ul>	Hyndman and Koehler, 2006
$R^2 = 1 - \frac{\sum_{i=1}^n (y_i - \hat{y}_i)^2}{\sum_{i=1}^n (y_i - \bar{y})^2}$	<ul style="list-style-type: none"> <li>Represents the proportion of variance in the dependent variable that can be explained by the independent variables.</li> <li>Values closer to 1 indicate a better fit</li> </ul>	Darlington, 1990; Chicco et al., 2021

313 *\* $y_i$  and  $\hat{y}_i$  representing the actual and predicted value and,  $\bar{y}$  and  $n$  standing for the mean of actual value and number of*  
 314 *observations in the dataset, respectively.*

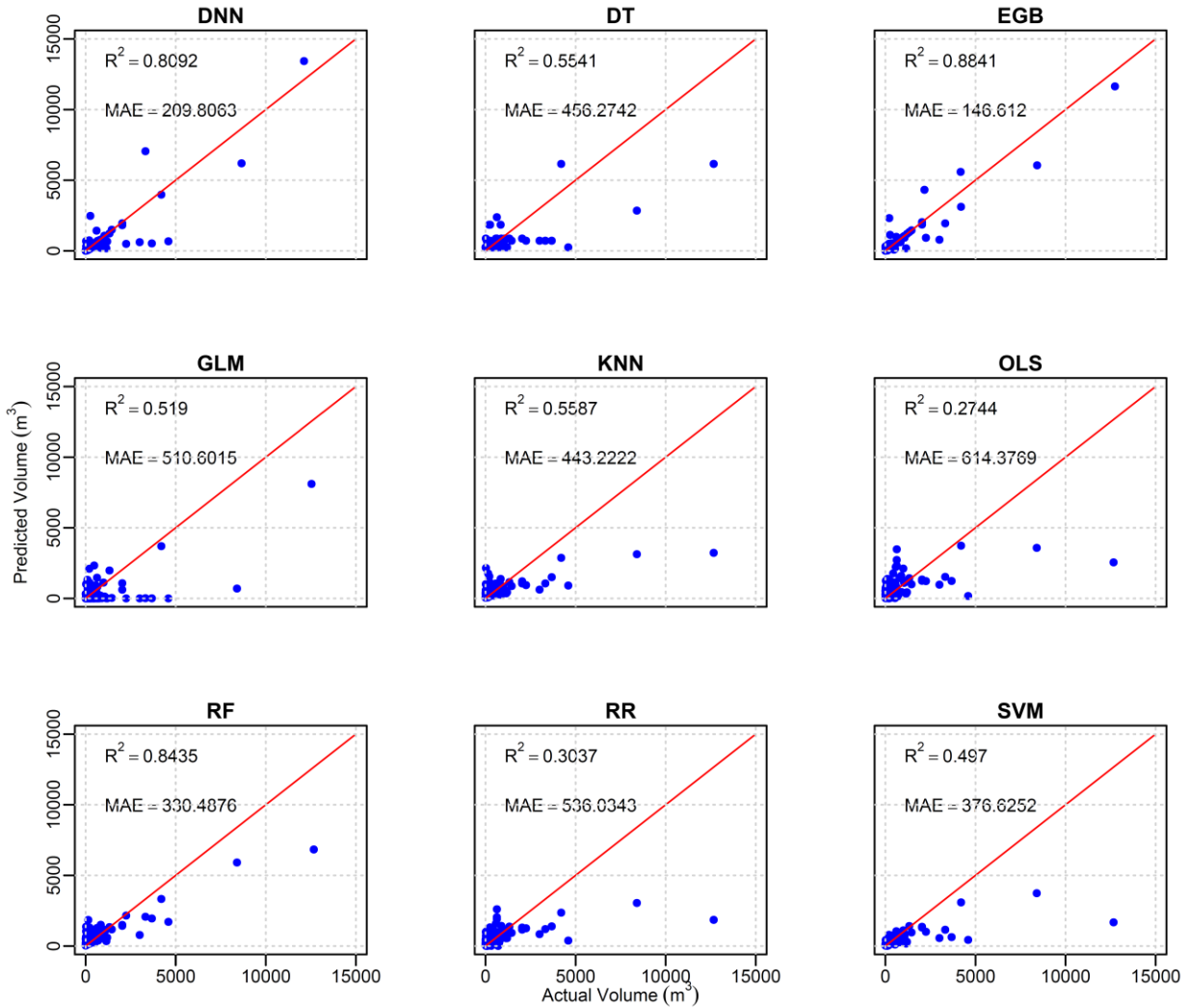
315

316 **4. Results**

317 This section details how all analyses and model development were performed in R using various libraries.  
 318 The DNN regression model was constructed using `dnn()` function from the `cito` library (Amesoeuer et al., 2023), with  
 319 two hidden layers of (50, 50) nodes. The model was trained on 1500L epochs, learning rate ( $lr = 0.01$ ), and loss =  
 320 "mae". The DT regression model was constructed with `tree()` function from the `tree` library, with the recursive-partition  
 321 method. The RR model was constructed using `glmnet()` from the `glmnet` package (Friedman et al., 2010), with ridge  
 322 penalty ( $\alpha=0$ ). The optimal lambda was obtained by performing 10-fold cross-validation. The EGB model was  
 323 built using `xgboost()` function in `xgboost` package (Chen et al., 2022). The optimal model was obtained at 524<sup>th</sup>  
 324 boosting iteration with max depth =5 and other parameters set to default. The GLM regression model was constructed

325 using `glm()` function (R core Team, 2022) with family Gaussian and log link to constrain the model of predicting  
326 positive outcomes. The KNN regression was constructed using `knnreg()` function from the `caret` package (Kuhn, 2022),  
327 with number of neighbors,  $k=17$ . The OLS model was constructed `lm()` from the `stats` package (R core Team, 2022).  
328 The RF model was run using `randomForest()` from the `randomforest` package (Liaw and Wiener, 2002) with default  
329 parameters and the optimal model was reached at 256<sup>th</sup> iteration. The SVM regression model with linear kernel was  
330 built using `e1071` package (Meyer et al., 2021) and other parameters set to default.

331 The predictive performance of all tested models on the holdout dataset is depicted by the scatterplot (Fig. 5)  
332 of actual volume as recorded in the test set and predicted outcome values of each model. The red line represents the  
333 perfect prediction. The scatter plot of actual and predicted values of tested models shows that OLS performed least  
334 compared to other models with  $R^2=0.2744$ , that is, 27% of variances in the model were explained by predictors. The  
335 second least performing was the RR with  $R^2= 0.3034$ , which is 3.6% improvement compared to OLS. Among all  
336 models, three out of nine, namely, OLS, SVM, and RR, performed below 50%; however, these models predicted well  
337 small values of volume (below 2000m<sup>3</sup>). The MAE of these three models was higher than the remaining six models,  
338 namely DNN, DT, GLM, KNN, RF, and EGB. Among these lasts, the most performing was EGB with  $R^2= 0.88$  of  
339 variance explained by predictors and MAE=146.6 m<sup>3</sup>. The evaluation metrics for the training and tested models are  
340 summarized in Table 4. Considering the  $R^2$ , the three models, namely EGB, RF, and DNN, had a value of  $R^2$  above  
341 80% on the holdout set.



342

343 **Figure 5: Scatterplot of actual and predicted values for the nine tested models.**

344

345 Regarding the prediction on the training set, the GLM had an  $R^2$  of 83%. Nevertheless, the prediction on the  
 346 holdout set was 51.9%; this large variation in variance explained by predictors indicates that the GLM model did not  
 347 catch all non-linear patterns in the holdout set. Notably, the prediction difference in  $R^2$  on both training and test for  
 348 the random forest exhibited a very small difference compared to EGB and DNN, that is, 1.75% compared to 12.17%  
 349 and 7.72% for DNN and EGB, respectively. Despite the stable prediction of RF, the performance in terms of SMAPE,  
 350 the DNN was the second lowest symmetric mean absolute percentage error, 43.83m<sup>3</sup> and 39.79 m<sup>3</sup> on training and test  
 351 sets, respectively. According to Chicco et al. (2021), the  $R^2$  is more informative in regression modeling; thus, RF had  
 352 better predictions than the DNN.

353

354

355

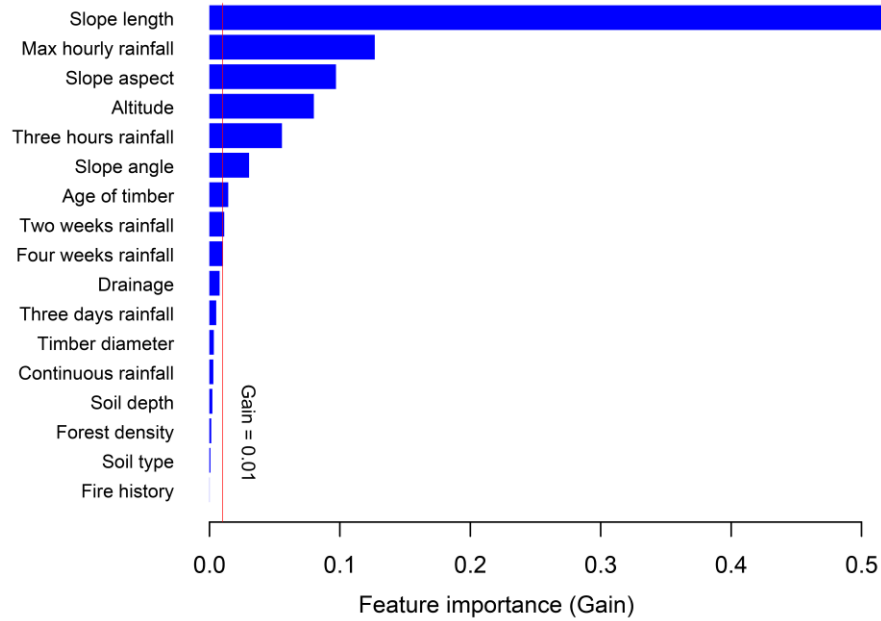


356 **Table 4: Summary of prediction metrics for tested models on the training and test set.**

Metrics		Models								
		DNN	DT	EGB	GLM	KNN	OLS	RF	RR	SVM
R <sup>2</sup>	Train	0.9309	0.4514	0.9613	0.8380	0.3470	0.3775	0.8610	0.3382	0.5510
	Test	0.8092	0.5822	0.8841	0.5190	0.5587	0.2744	0.8435	0.3037	0.4970
MAE	Train	132.7429	407.0814	75.1250	308.9700	410.2945	502.0053	236.9516	470.1633	276.2000
	Test	209.8063	435.5836	146.6120	510.6015	443.2222	614.3769	330.4876	536.0343	376.6252
RMSE	Train	348.6190	940.4850	113.4940	570.0070	1027.3730	1001.7620	574.9720	1042.9110	916.5471
	Test	646.5438	1047.4880	501.8960	1055.9190	1115.5270	1234.1220	737.0857	1237.9420	1176.9410
MAPE	Train	0.5240	0.7930	0.1540	76.3530	0.6280	5.2310	0.3810	1.5330	1.1588
	Test	0.5623	0.8892	0.3132	1819.2220	0.6623	4.1277	0.4939	5.8428	1.0421
SMAPE	Train	43.8375	79.8680	13.1780	150.4262	67.4715	103.0555	52.3359	93.4002	67.3221
	Test	39.7998	81.4539	22.7237	152.4991	73.6498	106.9756	63.7582	93.9244	76.9794

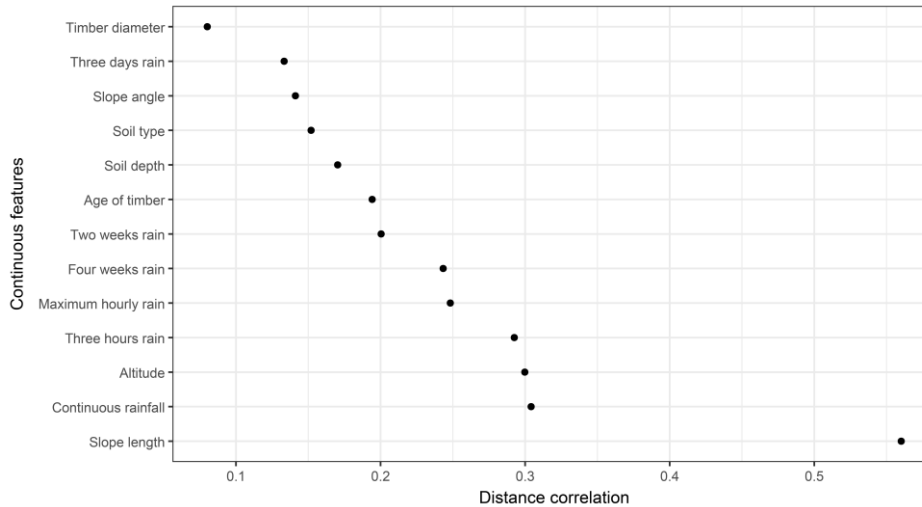
357

358 To dive deep into the prediction performance of the EGB model, we analyzed variables importance in the  
359 prediction of the volume. It was observed that slope length was the most contributing predictor in the performance of  
360 the EGB model, followed by maximum hourly rainfall and slope aspect. The altitude, three hours rainfall, slope angle  
361 and age of timber contributed moderately to the prediction of the outcome volumes with gain above 0.01 and less than  
362 0.2. The antecedent rainfall from three days and above and continuous rainfall had a minor contribution, with a gain  
363 of less than 0.01 for each. The presence of rainwater drainage channels had a moderate contribution, with a gain close  
364 to 0.01. On the other hand, the contribution of soil depth and forest density in the models was insignificant and far  
365 below 0.01. Though Figure 2(a) depicted the association between larger volumes and fire history, the variable  
366 importance indicates that the relation was not significant. Even though some variables had minor contributions,  
367 depending on the case, the contribution of those variables may also increase depending on other regional settings.  
368 Therefore, all variables with GVIF below 10 were kept in the model. Figure 6 illustrates the variables importance for  
369 the EGB model. The vertical red line splits landslides prediction features into two groups, the first containing features  
370 that contributed a gain above 0.01 and others with minor contributions.



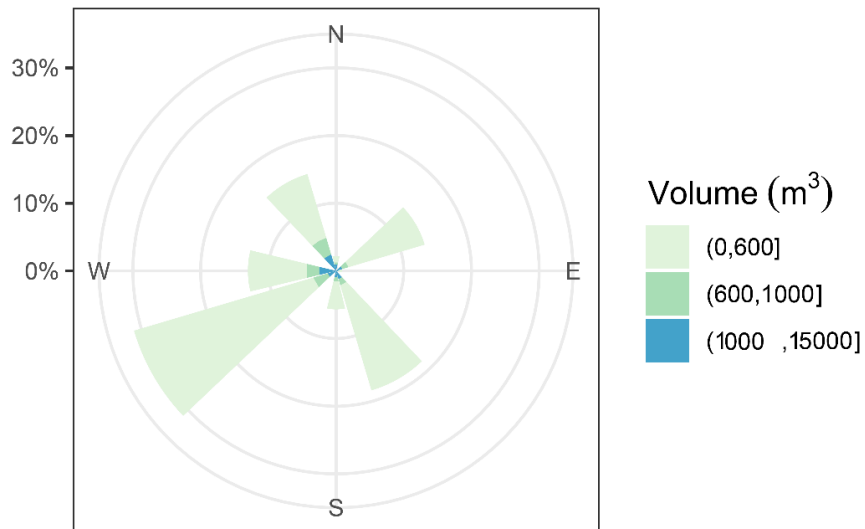
371  
 372 **Figure 6: Variable importance for the EGB model.**

373  
 374 The variable importance plot depicts the overall contribution of a given feature; however, it does not provide  
 375 detailed information. To get more insight into the relationship between the volume of landslides and predictors,  
 376 statistical tests for normality, namely, Shapiro-Wilk’s test, and Dunn’s test were conducted. The Shapiro-Wilk’s test  
 377 (Dudley, 2023) results revealed that the distribution of volume was non-normal ( $W = 0.40642$ ,  $p\text{-value} < 0.001$ ).  
 378 Noting that the volume distribution was non-normal, we opted for the non-parametric tests, which do not rely on  
 379 normality to conduct the distance correlation (Székely et al., 2007) test (dcor) for continuous independent features.  
 380 Figure 7 illustrates that the slope length exhibited a higher value ( $dcor=0.56$ ) followed by continuous rainfall altitude  
 381 and three hours rainfall and kept decreasing up to timber diameter with a distance correlation of 0.08. Overall, the  
 382 distance correlation between the volume of landslides shows a moderate strength of association between continuous  
 383 predictors.  
 384



385  
386 **Figure 7: Distance correlation plot for the volume and continuous features.**

387  
388 Furthermore, to test for categorical features, Kruskal-Wallis test (McKight and Najab, 2010) was used to  
389 check whether the volume of the landslide was different in each category and Dunn's tests (Dinno, 2015) were applied  
390 to examine which categories had similar means of the volume of landslides due to rainfall in different categories. The  
391  $H_0$  (null hypothesis) was that the mean volume of landslides in different categories is the same, and the  $H_1$  (alternative  
392 hypothesis) was that the means of landslides are different in some categories. For the slope aspect, the second most  
393 significant predictor for the EGB model, the results of Kruskal-Wallis test (chi-squared = 20.889,  $df = 7$ ,  $p$ -value =  
394 0.003938) showed that there is a significant difference in median of volume in some categories of slope aspects. To  
395 know which classes of slope aspects had significantly different mean volumes, the Dunn's test results at 95%  
396 confidence interval, pairs (East-South west, East-South East, East-South, East-North West and North West-South East)  
397 had significantly different means of landslides' volume (with  $p$ -value <0.05). Figure 8 depicts that the southwest and  
398 southeast aspects had a higher frequency of landslides.



399  
400 **Figure 8: The distribution of the volume of landslides due to rainfall with respect to the slope aspect.**

401  
402  
403  
404  
405  
406  
407  
408  
409  
410  
411  
412  
413  
414  
415  
416  
417  
418  
419  
420  
421  
422  
423  
424  
425  
426  
427  
428  
429  
430  
431  
432  
433  
434  
435  
436  
437

The Kruskal-Wallis test for the difference in mean of drainage classes showed the result was: chi-squared = 15.792, df = 2, p-value = 0.000372, which shows that the means of volume per class were different. This was clarified by Dunn's test results, p-values were less than 0.05 in all pairwise mean difference comparisons. The results of these tests highlighted that drainage has a remarkable influence on the occurrence of rainfall-induced landslides in the Korean Peninsula.

## 5. Discussion

Numerical models have traditionally been employed due to their foundation in physical principles such as slope stability and hydrological dynamics (Glade et al., 2005). These models are valuable for understanding the underlying mechanisms of landslide processes but often face limitations when applied to regions with complex or heterogeneous terrain, as they require detailed, high-quality input data that may not always be available (Caine, 1980). In the same way, statistical models, which use historical rainfall and landslide data to establish correlations, can offer useful predictions of VLDR in regions with extensive historical records (Chung and Fabbri, 2003). However, these models may struggle to account for local variations in topography or rapidly changing weather patterns, limiting their general applicability. Additionally, ML techniques have shown significant promise in improving predictive accuracy at the regional level due to the capability of processing large, diverse datasets and capturing complex, non-linear relationships that traditional models might fail to capture (Pourghasemi and Rahmati, 2018). Further, ML models can adapt to regional variations and continuously improve as new data is introduced, offering a more flexible and dynamic approach to predict VLDR on a regional scale (Liu et al., 2021b). Subsequently, the aim of this study was to construct a data-driven algorithm that accurately predicts the VLDR. The result of nine different tested algorithms revealed a tremendous difference between classical regression models (OLS, RR, and GLM) and other data-driven machine learning models. In this study, apart from SVM regression, DT and KNN, other machine learning models (DNN, DT, RF, and EGB) exhibited high prediction capability with  $R^2$  above 50% (Fig. 5). The DNN, EGB, and RF models achieved  $R^2 > 0.8$  on both training and test set with accuracy reduced  $R^2$  by 1.75, 7.72, and 12.17% for RF, EGB and DNN respectively, on the holdout set, indicating that the model could yield reliable volume estimates in adjacent areas with similar geological and environmental conditions. The random forest model performed well in predicting smaller volume; however, as the volume increased, the model underpredicted volume values. The DNN model performed quite well with low MAE compared to random forest; however, the model did not perform well on moderate volume values, resulting in reduced  $R^2$ . The EGB model tested on South Korean landslide inventory coupled with rainfall data at the time of landslide events and antecedent rainfall within one month of the event exhibited more accurate predictions compared to other constructed algorithms. The difference in performance may be due to the internal structure of each algorithm; the RF builds multiple decision trees and averages predictions to improve accuracy (Breiman, 2001), while the EGB builds sequential trees in a recursive order where the new built tree improves error occurred while building the previous decision tree and optimizes the loss function through a gradient descent (Chen et al., 2022).

The slope aspect played an important role in the prediction of the volume, and the landslide mostly occurred

438 in locations oriented toward south-southwest and southeast. That may be due to the direction taken by typhoons, which  
439 hit the southwest versants of mountains upon landfall on the Korean peninsula toward the North East Pacific (Lee et  
440 al., 2013; Ha, 2022). The findings of this research are congruent with those of Lee et al. (2013), who also highlighted  
441 that the mountain versant oriented to strong wind direction may face more landslides. The study also highlighted that  
442 a moderate rainwater drainage channel plays an important role in the prevention of landslides due to its stabilizing  
443 effect. The landslide location and pattern follow the rainfall climate scenario, which highlighted a higher intensity of  
444 rainfall in the northeastern region of South Korea (Lee, 2016). In addition, the findings of this study are congruent  
445 with Zhang et al. (2019) observations that highlighted the low influence of soil type in landslide modeling and the  
446 maximum rainfall and cumulative three hours of rainfall were the most contributing rainfall, which indicated that these  
447 shallow landslides may have been triggered by sudden rainfall concentrated in few hours before the occurrence of the  
448 event. The occurrence of landslides triggered by rainfall is a complex phenomenon that involves many interrelated  
449 environmental settings, human activity, geological conditions and climatic conditions. Moreover, the occurrence of  
450 typhoons is known to aggravate the landslides impacts on communities (Chang et al., 2008); incorporating typhoon  
451 variables in future studies to customize for regional settings may improve the accuracy of the model. The advantage  
452 of his research is that the constructed model has high predictive accuracy and can handle the non-linearity of  
453 predisposing factors. The model came to fill the gap in a few literatures related to the prediction of the volume of  
454 landslides using data-driven techniques. This model can serve as an effective tool for policy-makers to incorporate  
455 landslide volume risks into policies aimed at protecting infrastructure and residents dwelling in landslides high risks  
456 zones.

457 To understand the applicability of the developed models, the trained model was tested using unknown data  
458 (test data), with volume predictions generated solely based on the predictor variables; actual volume values were  
459 utilized only for evaluating model prediction accuracy. The outcome exhibited that the difference in  $R^2$  on the training  
460 and holdout set of 7.72% for the optimal model (i.e., EGB) highlights that the model can be applied to another region  
461 of a similar setting. It was noted that without proper model calibration with the independent data set, it's difficult to  
462 determine whether these discrepancies in performance are due to model limitations or data differences in different  
463 regions (Huang et al., 2020). Therefore, future research will focus on developing an independent database containing  
464 recent landslide geometry data from various regions of the Korean Peninsula to enhance model accuracy, along with  
465 calibrating region-specific parameters to ensure the model's transferability to other regions.

466 The major limitation of this study is that the analysis is solely focused on shallow-seated landslides,  
467 specifically translational slope failures with volumes below 13,000m<sup>3</sup>. Thus, the analysis may not fully capture the  
468 variability in landslide characteristics across different geomorphological and geological contexts. Deep-seated  
469 landslides, for instance, often exhibit distinct failure mechanisms, material compositions, and depositional patterns  
470 that influence their volumetric characteristics, which were not considered in this investigation. Similarly, debris flows,  
471 known for their unique channelization and entrainment behaviors, were not included, potentially limiting the  
472 applicability of the optimized models to other landslide types. Further, this study was also performed using point-  
473 based landslide inventory data, which may not capture all variability of influencing factors and their exact state. The  
474 incorporation of high-resolution data from remote sensing and other sources may also improve the efficiency of the

475 predictions. These limitations may impact the broader applicability of the proposed model; however, future studies  
476 will aim to address this by conducting separate analyses for deep-seated landslides and debris flows, allowing for a  
477 more comprehensive understanding of landslide volume predictions across diverse landslide types and  
478 geomorphological settings.

479

## 480 **6. Conclusions**

481 In this paper, the aim was to construct a data-driven model that predicts the volume of landslides due to rainfall. To  
482 this, nine different classical regression models and machine learning algorithms were tested on South Korean landslide  
483 data set containing features of landslides that occurred between 2011 and 2012. Among the tested models, the EGB  
484 model produced the most accurate prediction. This is proven by the evaluation of the difference between actual and  
485 predicted values, such as  $R^2= 88.41\%$  and  $MAE=146.6120m^3$  on the holdout set. The analysis of feature variables in  
486 the contribution to the prediction of the model revealed that the slope length was the most influencing predictor. The  
487 EGB model can be a promising tool for the prediction of the volume of landslides due to its high predictive  
488 performance. The model can be customized in different environmental settings. The model can be applied to estimate  
489 the expected volume of landslides based on forecasted rainfall once the model is well-adjusted to fit the  
490 geomorphological and environmental settings of the region of interest after re-training on the regional historical data  
491 to include regional variability. Therefore, this model can be a good tool for planning for resilience and infrastructure  
492 pre-construction risk assessment to ensure the new infrastructure is placed in stable regions free from severe landslides.

493

## 494 **Acknowledgments**

495 This research was supported by the Korean government (MSIT) (2021R1C1C2003316) and Basic Science Research  
496 Program through the National Research Foundation of Korea (NRF) funded by Ministry of Education  
497 (2021R1A6A1A03044326). The authors highly appreciate both anonymous reviewers and editor for their constructive  
498 suggestions that helped us improve the preprint version.

499

## 500 **Code availability**

501 The codes used forVDLR prediction are available from the corresponding author upon reasonable request.

502

## 503 **Data availability**

504 All data used in this study are available from the corresponding author upon request.

505

## 506 **Author contributions**

507 TJ: conceptualization, formal analysis, investigation, methodology, software/code, data curation, visualization,  
508 validation, and writing (original draft preparation and review and editing). CYN: data curation, supervision, and writing  
509 (review and editing). GK: data curation, supervision, and writing (review and editing). SWL: data curation, supervision,  
510 and writing (review and editing). MDA: conceptualization, formal analysis, investigation, methodology, software,  
511 data curation, visualization, validation, and writing (original draft preparation and review and editing). SGY:

512 conceptualization, investigation, supervision, methodology, project administration, and writing (review and editing).

513

#### 514 **Competing interests**

515 The contact author has declared that none of the authors has any competing interests.

516

#### 517 **References**

518 Alcántara, A. L., and Ahn, K. H.: Probability distribution and characterization of daily precipitation related to tropical  
519 cyclones over the Korean Peninsula, *Water*, 12(4), 1214, <https://doi.org/10.3390/w12041214>, 2020.

520 Alcántara-Ayala, I., and Sassa, K.: Landslide risk management: from hazard to disaster risk reduction, *Landslides*,  
521 20(10), 2031-2037, <https://doi.org/10.1007/s10346-023-02140-5>, 2023.

522 Amesoder, C., Hartig, F., and Pichler, M.: cito: An R package for training neural networks using torch, arXiv e-prints,  
523 arXiv-2303, <https://doi.org/10.1111/ecog.07143>, 2023.

524 Armstrong, J. S.: Combining forecasts (pp. 417-439), Springer US, [https://doi.org/10.1007/978-0-306-47630-3\\_19](https://doi.org/10.1007/978-0-306-47630-3_19),  
525 2001.

526 Asada, H., and Minagawa, T.: Impact of vegetation differences on shallow landslides: a case study in Aso, Japan,  
527 *Water*, 15(18), 3193, <https://doi.org/10.3390/w15183193>, 2023.

528 Bernardie, S., Desramaut, N., Malet, J.-P., Gourlay, M., and Grandjean, G.: Prediction of changes in landslide rates  
529 induced by rainfall, *Landslides*, 12(3), 481-494, <https://doi.org/10.1007/s10346-014-0495-8>, 2014.

530 Bonamutial, M., and Prasetyo, S. Y.: Exploring the Impact of Feature Data Normalization and Standardization on  
531 Regression Models for Smartphone Price Prediction, In 2023 International Conference on Information  
532 Management and Technology (ICIMTech) (pp. 294-298), IEEE,  
533 <https://doi.org/10.1109/ICIMTech59029.2023.10277860>, 2023.

534 Borup, D., Christensen, B. J., Mühlbach, N. S., and Nielsen, M. S.: Targeting predictors in random forest regression,  
535 *Int. J. Forecast.*, 39(2), 841-868, <https://doi.org/10.1016/j.ijforecast.2022.02.010>, 2023.

536 Breiman, L.: Random forests, *Machine Learning*, 45, 5-32, <https://doi.org/10.1023/A:1010933404324>, 2001.

537 Breiman, L.: Classification and regression trees, Routledge, <https://doi.org/10.1201/9781315139470>, 2017.

538 Caine, N.: The rainfall intensity-duration control of shallow landslides and debris flows, *Geografiska annaler: series*  
539 *A, Phys. Geogr.*, 62(1-2), 23-27, <https://doi.org/10.1080/04353676.1980.11879996>, 1980.

540 Celtek, S.: The effect of aspect on landslide and its relationship with other parameters, In *Landslides*, IntechOpen.,  
541 <https://dx.doi.org/10.5772/intechopen.99389>, 2021.

542 Chang, K. T., and Chiang, S. H.: An integrated model for predicting rainfall-induced landslides, *Geomorphology*,  
543 105(3-4), 366-373, <https://doi.org/10.1016/j.geomorph.2008.10.012>, 2009.

544 Chang, K. T., Chiang, S. H., and Lei, F.: Analysing the relationship between typhoon-triggered landslides and critical  
545 rainfall conditions, *Earth Surf. Process. Landf.: J. British Geomor. Res. Group*, 33(8), 1261-1271,  
546 <https://doi.org/10.1002/esp.1611>, 2008.

547 Chatra, A. S., Dodagoudar, G. R., and Maji, V. B.: Numerical modelling of rainfall effects on the stability of soil  
548 slopes, *Int. J. Geotech. Eng.*, <https://doi.org/10.1080/19386362.2017.1359912>, 2019.

549 Chen, T., He, T., Benesty, M., Khotilovich, V., Tang, Y., Cho, H., Chen, K., Mitchell, R., Cano, I., Zhou, T., Li, M.,  
550 Xie, J., Lin, M., Geng, Y., Li, Y., and Yuan, J.: xgboost: Extreme Gradient Boosting, R package version  
551 1.6.0.1, <https://CRAN.R-project.org/package=xgboost>, last access: 25 January 2025, 2022.

552 Chen, C. W., Oguchi, T., Hayakawa, Y. S., Saito, H., and Chen, H.: Relationship between landslide size and rainfall  
553 conditions in Taiwan, *Landslides*, 14, 1235-1240, <https://doi.org/10.1007/s10346-016-0790-7>, 2017.

554 Chen, L., Guo, Z., Yin, K., Shrestha, D. P., and Jin, S.: The influence of land use and land cover change on landslide  
555 susceptibility: a case study in Zhushan Town, Xuan'en County (Hubei, China), *Nat. Hazards Earth Syst.*  
556 *Sci.*, 19(10), 2207-2228, <https://doi.org/10.5194/nhess-19-2207-2019>, 2019.

557 Chen, X., Zhang, L., Zhang, L., Zhou, Y., Ye, G., and Guo, N.: Modelling rainfall-induced landslides from initiation  
558 of instability to post-failure, *Comput. Geotech.*, 129, 103877,  
559 <https://doi.org/10.1016/j.compgeo.2020.103877>, 2021.

560 Chen, Z., Luo, R., Huang, Z., Tu, W., Chen, J., Li, W., Chen, S., Xiao, J. and Ai, Y.: Effects of different backfill soils  
561 on artificial soil quality for cut slope revegetation: Soil structure, soil erosion, moisture retention and soil  
562 C stock, *Ecol. Eng.*, 83, 5-12, <https://doi.org/10.1016/j.ecoleng.2015.05.048>, 2015.

563 Cheung, R. W.: Landslide risk management in Hong Kong, *Landslides*, 18(10), 3457-3473,  
564 <https://doi.org/10.1007/s10346-020-01587-0>, 2021.

565 Chicco, D., Warrens, M. J., and Jurman, G.: The coefficient of determination R-squared is more informative than  
566 SMAPE, MAE, MAPE, MSE and RMSE in regression analysis evaluation, *PeerJ Comput. Sci.*, 7, e623,  
567 <https://doi.org/10.7717/peerj-cs.623>, 2021.

568 Chowdhury, M. Z. I., Leung, A. A., Walker, R. L., Sikdar, K. C., O’Beirne, M., Quan, H., and Turin, T. C.: A  
569 comparison of machine learning algorithms and traditional regression-based statistical modeling for  
570 predicting hypertension incidence in a Canadian population, *Sci. Rep.*, 13(1), 13,  
571 <https://doi.org/10.1038/s41598-022-27264-x>, 2023.

572 Chung, C. J. F., and Fabbri, A. G.: Validation of spatial prediction models for landslide hazard mapping, *Nat. Hazards*,  
573 30, 451-472, <https://doi.org/10.1023/B:NHAZ.0000007172.62651.2b>, 2003.

574 Cohen, D., and Schwarz, M.: Tree-root control of shallow landslides, *Earth Surf. Dyn.*, 5(3), 451-477,  
575 <https://doi.org/10.5194/esurf-5-451-2017>, 2017.

576 Culler, E. S., Livneh, B., Rajagopalan, B., and Tiampo, K. F.: A data-driven evaluation of post-fire landslide  
577 susceptibility, *Nat. Hazards Earth Syst. Sci.*, 2021, 1-24, <https://doi.org/10.5194/nhess-23-1631-2023>,  
578 2021.

579 Dahal, B. K., and Dahal, R. K.: Landslide hazard map: tool for optimization of low-cost mitigation, *Geoenvironmental*  
580 *Disasters*, 4, 1-9, <https://doi.org/10.1186/s40677-017-0071-3>, 2017.

581 Dai, F. C., and Lee, C. F.: Frequency–volume relation and prediction of rainfall-induced landslides, *Eng. Geol.*, 59(3-  
582 4), 253-266, [https://doi.org/10.1016/S0013-7952\(00\)00077-6](https://doi.org/10.1016/S0013-7952(00)00077-6), 2001.

583 Darlington, R. B.: *Regression and linear models*, McGraw-Hill, New York, USA, ISBN: 0070153728, 9780070153721,  
584 1990.

585 Dinno, A.: Nonparametric pairwise multiple comparisons in independent groups using Dunn's test, *Stata J.*, 15(1),  
586 292-300, <https://doi.org/10.1177/1536867X1501500117>, 2015.

587 Dobson, A. J., and Barnett, A. G.: *An introduction to generalized linear models*, CRC press, New York, USA, ISBN:  
588 9781315182780, <https://doi.org/10.1201/9781315182780>, 2018.

589 Donnarumma, A., Revellino, P., Grelle, G., and Guadagno, F. M.: Slope angle as indicator parameter of landslide  
590 susceptibility in a geologically complex area, *Landslide Science and Practice: Volume 1: Landslide*  
591 *Inventory and Susceptibility and Hazard Zoning*, 425-433, Springer, Berlin , [https://doi.org/10.1007/978-](https://doi.org/10.1007/978-3-642-31325-7_56)  
592 [3-642-31325-7\\_56](https://doi.org/10.1007/978-3-642-31325-7_56), 2013.

593 Duc, D. M.: Rainfall-triggered large landslides on 15 December 2005 in Van Canh district, Binh Dinh province,  
594 Vietnam, *Landslides*, 10(2), 219-230. <https://doi.org/10.1007/s10346-012-0362-4>, 2013.

595 Dudley, R.: The Shapiro–Wilk test for normality, Available at <https://math.mit.edu/~rmd/46512/shapiro.pdf> , last  
596 access: 25 January 2025, 2023.

597 Evans, S., Mugnozza, G.S., Strom, A., Hermanns, R., Ischuk, A., Vinnichenko, S.: Landslides From Massive Rock  
598 Slope Failure And Associated Phenomena, In: *Landslides from Massive Rock Slope Failure*, NATO  
599 Science Series, vol 49, Springer, Dordrecht., [https://doi.org/10.1007/978-1-4020-4037-5\\_1](https://doi.org/10.1007/978-1-4020-4037-5_1), 2006.

600 Friedman, J. H., Hastie, T., and Tibshirani, R.: Regularization paths for generalized linear models via coordinate  
601 descent, *J. Stat. Softw.*, 33, 1-22, Available at <https://pmc.ncbi.nlm.nih.gov/articles/PMC2929880/>, last  
602 access: 25 January 2025, 2010.

603 Gariano, S. L., Rianna, G., Petrucci, O., and Guzzetti, F.: Assessing future changes in the occurrence of rainfall-  
604 induced landslides at a regional scale, *Sci. Total Environ.*, 596, 417-426,  
605 <https://doi.org/10.1016/j.scitotenv.2017.03.103>, 2017.



606 Gelman, A., and Hill, J.: Data analysis using regression and multilevel/hierarchical models, Cambridge University  
607 Press, New York, ISBN: 0-521-86706-1, 2007.

608 Glade, T., Anderson, M. G., and Crozier, M. J.: Landslide hazard and risk (Vol. 807), John Wiley & Sons, ISBN:  
609 9780470012659, <https://doi.org/10.1002/9780470012659>, 2005.

610 Gong, Q., Wang, J., Zhou, P., and Guo, M.: A regional landslide stability analysis method under the combined impact  
611 of rainfall and vegetation roots in south China, *Adv. Civ. Eng.*, 1-12, <https://doi.org/10.1155/2021/5512281>,  
612 2021.

613 Gonzalez-Ollauri, A., and Mickovski, S. B.: Hydrological effect of vegetation against rainfall-induced landslides, *J.*  
614 *Hydrol.*, 549, 374-387. <https://doi.org/10.1016/j.jhydrol.2017.04.014>, 2017.

615 Greenwood, J. R., Norris, J. E., and Wint, J.: Assessing the contribution of vegetation to slope stability, *Proc. Inst.*  
616 *Civil Eng. Geotech. Eng.*, 157(4), 199-207, <https://doi.org/10.1680/geng.2004.157.4.199>, 2004.

617 Gutierrez-Martin, A.: A GIS-physically-based emergency methodology for predicting rainfall-induced shallow  
618 landslide zonation, *Geomorphology*, 359, 107121, <https://doi.org/10.1016/j.geomorph.2020.107121>, 2020.

619 Guzzetti, F., Peruccacci, S., Rossi, M., and Stark, C. P.: The rainfall intensity–duration control of shallow landslides  
620 and debris flows: an update, *Landslides*, 5, 3-17, <https://doi.org/10.1007/s10346-007-0112-1>, 2008.

621 Ha, K. M.: Predicting typhoon tracks around Korea, *Nat. Hazards*, 113(2), 1385-1390, <https://doi.org/10.1007/s11069-022-05335-6>, 2022.

623 Hastie, T.: The elements of statistical learning: data mining, inference, and prediction, 2nd edition, Springer, New  
624 York, <https://doi.org/10.1111/j.1541-0420.2010.01516.x>, ISBN: 9780387848570, 2009.

625 Highland, L. and Bobrowsky, P.: The Landslide Handbook: A Guide to Understanding Landslides, USGS, Reston, VA,  
626 Circular 1325, Available at <https://pubs.usgs.gov/circ/1325/>, last access: 25 January 2025, 2008.

627 Holcombe, E. A., Beesley, M. E., Vardanega, P. J., and Sorbie, R.: Urbanisation and landslides: hazard drivers and  
628 better practices, In *Proc. Inst. Civ. Eng. Civ. Eng. (Vol. 169(3), pp. 137-144)*, Thomas Telford Ltd,  
629 <https://doi.org/10.1680/jcien.15.00044>, 2016.

630 Hovius, N., Stark, C. P., and Allen, P. A.: Sediment flux from a mountain belt derived by landslide mapping, *Geology*,  
631 25(3), 231-234, [https://doi.org/10.1130/0091-7613\(1997\)025<0231:SFFAMB>2.3.CO;2](https://doi.org/10.1130/0091-7613(1997)025<0231:SFFAMB>2.3.CO;2), 1997.

632 Huang, J., Hales, T. C., Huang, R., Ju, N., Li, Q., and Huang, Y.: A hybrid machine-learning model to estimate  
633 potential debris-flow volumes, *Geomorphology*, 367, 107333,  
634 <https://doi.org/10.1016/j.geomorph.2020.107333>, 2020.

635 Hyde, K. D., Riley, K., and Stoof, C.: Uncertainties in predicting debris flow hazards following wildfire, *Nat. Hazards*,  
636 <https://doi.org/10.1002/9781119028116.ch19>, 2016.

637 Hyndman, R. J., and Koehler, A. B.: Another look at measures of forecast accuracy, *Int. J. Forecast.*, 22(4), 679-688,  
638 <https://doi.org/10.1016/j.ijforecast.2006.03.001>, 2006.

639 Hyun, Y. K., Kar, S. K., Ha, K. J., and Lee, J. H.: Diurnal and spatial variabilities of monsoonal CG lightning and  
640 precipitation and their association with the synoptic weather conditions over South Korea, *Theor. Appl.*  
641 *Climatol.*, 102, 43-60, <https://doi.org/10.1007/s00704-009-0235-5>, 2010.

642 Intrieri, E., Carlà, T., and Gigli, G.: Forecasting the time of failure of landslides at slope-scale: A literature review,  
643 *Earth-Sci. Rev.*, 193, 333-349, <https://doi.org/10.1016/j.earscirev.2019.03.019>, 2019.

644 Jaboyedoff, M., Choffet, M., Derron, M. H., Horton, P., Loye, A., Longchamp, C., Mazotti, B., Michoud, C., and  
645 Pedrazzini, A.: Preliminary slope mass movement susceptibility mapping using DEM and LiDAR DEM, In  
646 *Terrigenous mass movements: Detection, modelling, early warning and mitigation using geoinformation*  
647 *technology*, 109-170, Springer, Berlin Heidelberg, [https://doi.org/10.1007/978-3-642-25495-6\\_5](https://doi.org/10.1007/978-3-642-25495-6_5), 2012.

648 Jin, H. G., Lee, H., and Baik, J. J.: Characteristics and possible mechanisms of diurnal variation of summertime  
649 precipitation in South Korea, *Theor. Appl. Climatol.*, 148(1), 551-568, <https://doi.org/10.1007/s00704-022-03965-1>, 2022.

651 Ju, L. Y., Zhang, L. M., and Xiao, T.: Power laws for accurate determination of landslide volume based on high-  
652 resolution LiDAR data, *Eng. Geol.*, 312, 106935, <https://doi.org/10.1016/j.enggeo.2022.106935>, 2023.

653 Jung, M. J., Jeong, Y. J., Shin, W. J., and Cheong, A. C. S.: Isotopic distribution of bioavailable Sr, Nd, and Pb in  
654 Chungcheongbuk-do Province, Korea, *J. anal. sci. technol.*, 15(1), 46, [https://doi.org/10.1186/s40543-024-](https://doi.org/10.1186/s40543-024-00460-2)  
655 [00460-2](https://doi.org/10.1186/s40543-024-00460-2), 2024.

656 Jung, Y., Shin, J. Y., Ahn, H., and Heo, J. H.: The spatial and temporal structure of extreme rainfall trends in South  
657 Korea, *Water*, 9(10), 809, <https://doi.org/10.3390/w9100809>, 2017.

658 Kafle, L., Xu, W. J., Zeng, S. Y., and Nagel, T.: A numerical investigation of slope stability influenced by the combined  
659 effects of reservoir water level fluctuations and precipitation: A case study of the Bianjiazhai landslide in  
660 China, *Eng. Geol.*, 297, 106508, <https://doi.org/10.1016/j.enggeo.2021.106508>, 2022.

661 Kang, M. W., Yibeltal, M., Kim, Y. H., Oh, S. J., Lee, J. C., Kwon, E. E., and Lee, S. S.: Enhancement of soil physical  
662 properties and soil water retention with biochar-based soil amendments, *Sci. Total Environ.*, 836, 155746,  
663 <https://doi.org/10.1016/j.scitotenv.2022.155746>, 2022.

664 Keefer, R. F.: *Handbook of soils for landscape architects*, Oxford University Press, ISBN: 0-19-51202-3, 2000.

665 Khan, M. A., Basharat, M., Riaz, M. T., Sarfraz, Y., Farooq, M., Khan, A. Y., Pham, Q. B., Ahmed, K. S., and Shahzad,  
666 A.: An integrated geotechnical and geophysical investigation of a catastrophic landslide in the Northeast  
667 Himalayas of Pakistan, *Geol. J.*, 56(9), 4760-4778, <https://doi.org/10.1002/gj.4209>, 2021.

668 Khan, Y. A., Lateh, H., Baten, M. A., and Kamil, A. A.: Critical antecedent rainfall conditions for shallow landslides  
669 in Chittagong City of Bangladesh, *Environmental Earth Sciences*, 67, 97-106.  
670 <https://doi.org/10.1007/s12665-011-1483-0>, 2012.

671 Kim, D. E., Seong, Y. B., Weber, J., and Yu, B. Y.: Unsteady migration of Taebaek Mountain drainage divide, Cenozoic  
672 extensional basin margin, Korean Peninsula, *Geomorphology*, 352, 107012,  
673 <https://doi.org/10.1016/j.geomorph.2019.107012>, 2020.

674 Kim, H. G., and Park, C. Y.: Landslide susceptibility analysis of photovoltaic power stations in Gangwon-do, Republic  
675 of Korea, *Geomat. Nat. Hazards Risk.*, 12(1), 2328-2351,  
676 <https://doi.org/10.1080/19475705.2021.1950219>, 2021.

677 Kim, J., Lee, K., Jeong, S., and Kim, G.: GIS-based prediction method of landslide susceptibility using a rainfall  
678 infiltration-groundwater flow model, *Eng. Geol.*, 182, 63-78,  
679 <https://doi.org/10.1016/j.enggeo.2014.09.001>, 2014.

680 Kim, M. S., Onda, Y., Kim, J. K., and Kim, S. W.: Effect of topography and soil parameterisation representing soil  
681 thicknesses on shallow landslide modelling, *Quat. Int.*, 384, 91-106,  
682 <https://doi.org/10.1016/j.quaint.2015.03.057>, 2015.

683 Kim, S. W., Chun, K. W., Kim, M., Catani, F., Choi, B., and Seo, J. I.: Effect of antecedent rainfall conditions and  
684 their variations on shallow landslide-triggering rainfall thresholds in South Korea, *Landslides*, 18, 569-  
685 582, <https://doi.org/10.1007/s10346-020-01505-4>, 2021.

686 Kitutu, M. G., Muwanga, A., Poesen, J., and Deckers, J. A.: Influence of soil properties on landslide occurrences in  
687 Bududa district, Eastern Uganda, *Afr. J. Agric. Res.*, 4(7), 611-620, Available at  
688 <https://lirias.kuleuven.be/retrieve/78489>, last access: 25 January 2025, 2009.

689 Korup, O.: Geomorphometric characteristics of New Zealand landslide dams, *Eng. Geol.*, 73(1-2), 13-35.  
690 <https://doi.org/10.1016/j.enggeo.2003.11.003>, 2004.

691 Korup, O., Clague, J. J., Hermanns, R. L., Hewitt, K., Strom, A. L., and Weidinger, J. T.: Giant landslides, topography,  
692 and erosion, *Earth Planet. Sci. Lett.*, 261(3-4), 578-589, <https://doi.org/10.1016/j.epsl.2007.07.025>, 2007.

693 Kotsakis, C.: Ordinary Least Squares, In *Encyclopedia of Mathematical Geosciences* (pp. 1032-1038), Cham:  
694 Springer, [https://doi.org/10.1007/978-3-030-85040-1\\_237](https://doi.org/10.1007/978-3-030-85040-1_237), 2023.

695 Kramer, O., and Kramer, O.: K-nearest neighbors, Dimensionality reduction with unsupervised nearest neighbors, 13-  
696 23, [https://doi.org/10.1007/978-3-642-38652-7\\_2](https://doi.org/10.1007/978-3-642-38652-7_2), 2013.

697 Krizhevsky, A., Sutskever, I., and Hinton, G. E.: Imagenet classification with deep convolutional neural networks,  
698 *Adv. Neural Inf. Process. Syst.*, 25, Available at  
699 [https://proceedings.neurips.cc/paper\\_files/paper/2012/file/c399862d3b9d6b76c8436e924a68c45b-](https://proceedings.neurips.cc/paper_files/paper/2012/file/c399862d3b9d6b76c8436e924a68c45b-Paper.pdf)  
700 [Paper.pdf](https://proceedings.neurips.cc/paper_files/paper/2012/file/c399862d3b9d6b76c8436e924a68c45b-Paper.pdf), last access: 25 January 2025, 2012.

701 Kuhn, M.: caret: Classification and Regression Training R package version 6.0-92, Available at [https://CRAN.R-](https://CRAN.R-project.org/package=caret)  
702 [project.org/package=caret](https://CRAN.R-project.org/package=caret), last access: 25 January 2025, 2022.

703 Kunz, M., and Kottmeier, C.: Orographic enhancement of precipitation over low mountain ranges, Part II: Simulations  
704 of heavy precipitation events over southwest Germany, *J. Appl. Meteorol. Clim.*, 45(8), 1041-1055,  
705 <https://doi.org/10.1175/JAM2390.1>, 2006.

706 Lacerda, W. A., Palmeira, E. M., Netto, A. L. C., and Ehrlich, M. (Eds.): Extreme rainfall induced landslides: an  
707 international perspective, Oficina de Textos, ISBN: 978-85-7975-150-9, 2014.

708 Lann, T., Bao, H., Lan, H., Zheng, H., and Yan, C.: Hydro-mechanical effects of vegetation on slope stability: A review,  
709 *Sci. Total Environ.*, 171691, <https://doi.org/10.1016/j.scitotenv.2024.171691>, 2024.

710 LeCun, Y., Bengio, Y., and Hinton, G.: Deep learning, *Nature*, 521(7553), 436-444,  
711 <https://doi.org/10.1038/nature14539>, 2015.

712 Lee, D. B., Kim, Y. N., Sonn, Y. K., and Kim, K. H.: Comparison of Soil Taxonomy (2022) and WRB (2022) Systems  
713 for classifying Paddy Soils with different drainage grades in South Korea, *Land*, 12(6), 1204,  
714 <https://doi.org/10.3390/land12061204>, 2023.

715 Lee, D. H., Cheon, E., Lim, H. H., Choi, S. K., Kim, Y. T., and Lee, S. R.: An artificial neural network model to predict  
716 debris-flow volumes caused by extreme rainfall in the central region of South Korea, *Eng. Geol.*, 281,  
717 105979, <https://doi.org/10.1016/j.enggeo.2020.105979>, 2021.

718 Lee, D. H., Kim, Y. T., and Lee, S. R.: Shallow landslide susceptibility models based on artificial neural networks  
719 considering the factor selection method and various non-linear activation functions, *J. Remote Sens.*, 12(7),  
720 1194, <https://doi.org/10.3390/rs12071194>, 2020.

721 Lee, J. U., Cho, Y. C., Kim, M., Jang, S. J., Lee, J., and Kim, S.: The effects of different geological conditions on  
722 landslide-triggering rainfall conditions in South Korea, *Water*, 14(13), 2051,  
723 <https://doi.org/10.3390/w14132051>, 2022.

724 Lee, M. J.: Rainfall and landslide correlation analysis and prediction of future rainfall base on climate change, In  
725 *Geohazards Caused by Human Activity*, IntechOpen, <https://dx.doi.org/10.5772/64694>, 2016.

726 Lee, S. W., Kim, G., Yune, C. Y., and Ryu, H. J.: Development of landslide-risk assessment model for mountainous  
727 regions in eastern Korea, *Disaster Adv.*, 6(6), 70-79, 2013.

728 Li, C. J., Guo, C. X., Yang, X. G., Li, H. B., and Zhou, J. W.: A GIS-based probabilistic analysis model for rainfall-  
729 induced shallow landslides in mountainous areas, *Environ. Earth Sci.*, 81(17), 432,  
730 <https://doi.org/10.1007/s12665-022-10562-y>, 2022.

731 Liaw, A., and Wiener, M.: Classification and regression by randomForest, *R News* 2(3), 18-22, Available at  
732 <https://journal.r-project.org/articles/RN-2002-022/RN-2002-022.pdf>, last access: 24 January 2025, 2002.

733 Liu, Y., Deng, Z., and Wang, X.: The effects of rainfall, soil type and slope on the processes and mechanisms of  
734 rainfall-induced shallow landslides, *Appl. Sci.*, 11(24), 11652, <https://doi.org/10.3390/app112411652>,  
735 2021a.

736 Liu, Z., Gilbert, G., Cepeda, J. M., Lysdahl, A. O. K., Piciullo, L., Hefre, H., and Lacasse, S.: Modelling of shallow  
737 landslides with machine learning algorithms, *Geosci. Front.*, 12(1), 385-393,  
738 <https://doi.org/10.1016/j.gsf.2020.04.014>, 2021b.

739 Luino, F., De Graff, J., Biddoccu, M., Faccini, F., Freppaz, M., Roccati, A., Ungaro, F., D'Amico, M., and Turconi,  
740 L.: The Role of soil type in triggering shallow landslides in the alps (Lombardy, Northern Italy), *Land*,  
741 11(8), <https://doi.org/10.3390/land11081125>, 2022.

742 Martinović, K., Gavin, K., Reale, C., and Mangan, C.: Rainfall thresholds as a landslide indicator for engineered  
743 slopes on the Irish Rail network, *Geomorphology*, 306, 40-50,  
744 <https://doi.org/10.1016/j.geomorph.2018.01.006>, 2018.

745 McKenna, J. P., Santi, P. M., Amblard, X., and Negri, J.: Effects of soil-engineering properties on the failure mode of  
746 shallow landslides, *Landslides*, 9, 215-228, <https://doi.org/10.1007/s10346-011-0295-3>, 2012.

747 McKight, P. E., and Najab, J.: Kruskal-wallis test, *The corsini encyclopedia of psychology*, 1-1,  
748 <https://doi.org/10.1002/9780470479216.corpsy0491>, 2010.

749 Meyer, D., Dimitriadou, E., Hornik, K., Weingessel, A., Leisch, F.: e1071: Misc Functions of the Department of  
750 Statistics, Probability Theory Group (Formerly: E1071), TU Wien R package version 1.7-9,  
751 <https://doi.org/10.32614/CRAN.package.e1071>, 2021.

752 Miao, F., Wu, Y., Xie, Y., and Li, Y.: Prediction of landslide displacement with step-like behavior based on  
753 multialgorithm optimization and a support vector regression model, *Landslides*, 15, 475-488,  
754 <https://doi.org/10.1007/s10346-017-0883-y>, 2018.

755 Montgomery, D. R., Schmidt, K. M., Dietrich, W. E., and McKean, J.: Instrumental record of debris flow initiation  
756 during natural rainfall: Implications for modeling slope stability, *J. Geophys. Res. Earth Surf.*, 114(F1),  
757 <https://doi.org/10.1029/2008JF001078>, 2009.

758 Nguyen, Q. H., Ly, H. B., Ho, L. S., Al-Ansari, N., Le, H. V., Tran, V. Q., Prakash, I., and Pham, B. T.: Influence of  
759 data splitting on performance of machine learning models in prediction of shear strength of soil, *Math.*  
760 *Probl. Eng.*, 2021(1), 4832864, <https://doi.org/10.1155/2021/4832864>, 2021.

761 O'brien, R. M.: A caution regarding rules of thumb for variance inflation factors, *Qual. Quant.*, 41, 673-690,  
762 <https://doi.org/10.1007/s11135-006-9018-6>, 2007.

763 Omwega, A. K.: Crop cover, rainfall energy and soil erosion in Githunguri (Kiambu District), Kenya, The University  
764 of Manchester (United Kingdom), Available at  
765 [https://www.proquest.com/openview/dd7c169f804775d18041ec262d03e4c1/1?cbl=2026366&diss=y&pq](https://www.proquest.com/openview/dd7c169f804775d18041ec262d03e4c1/1?cbl=2026366&diss=y&pq-origsite=gscholar)  
766 [-origsite=gscholar](https://www.proquest.com/openview/dd7c169f804775d18041ec262d03e4c1/1?cbl=2026366&diss=y&pq-origsite=gscholar), last access: 24 January 2025, 1989.

767 Panday, S., and Dong, J. J.: Topographical features of rainfall-triggered landslides in Mon State, Myanmar, August  
768 2019: Spatial distribution heterogeneity and uncommon large relative heights, *Landslides*, 18(12), 3875-  
769 3889, <https://doi.org/10.1007/s10346-021-01758-7>, 2021.

770 Park, C. Y.: The classification of extreme climate events in the Republic of Korea, *J. Korean Assoc. Regional Geograp.*,  
771 21(2), 394-410, Available at <https://koreascience.kr/article/JAKO201507740043627.page>, last access: 25  
772 January 2025, 2015.

773 Park, S. J., and Lee, D. K.: Predicting susceptibility to landslides under climate change impacts in metropolitan areas  
774 of South Korea using machine learning, *Geomat. Nat. Hazards Risk. and Risk*, 12(1), 2462-2476,  
775 <https://doi.org/10.1080/19475705.2021.1963328>, 2021.

776 Pham, B. T., Tien Bui, D., and Prakash, I.: Bagging based support vector machines for spatial prediction of landslides,  
777 *Environ. Earth Sci.*, 77, 1-17, <https://doi.org/10.1007/s12665-018-7268-y>, 2018.

778 Phillips, C., Hales, T., Smith, H., and Basher, L.: Shallow landslides and vegetation at the catchment scale: A  
779 perspective, *Ecol. Eng.*, 173, 106436. <https://doi.org/10.1016/j.ecoleng.2021.106436>, 2021.

780 Pisner, D. A., and Schnyer, D. M.: Support vector machine, In *Machine learning* (pp. 101-121), Academic Press,  
781 <https://doi.org/10.1016/B978-0-12-815739-8.00006-7>, 2020.

782 Pourghasemi, H. R., and Rahmati, O.: Prediction of the landslide susceptibility: Which algorithm, which precision?,  
783 *Catena*, 162, 177-192, <https://doi.org/10.1016/j.catena.2017.11.022>, 2018.

784 Qiu, H., Regmi, A. D., Cui, P., Cao, M., Lee, J., and Zhu, X.: Size distribution of loess slides in relation to local slope  
785 height within different slope morphologies, *Catena*, 145, 155-163,  
786 <https://doi.org/10.1016/j.catena.2016.06.005>, 2016.

787 R Core Team: R: A language and environment for statistical computing, R Foundation for Statistical Computing,  
788 Vienna, Austria, Available at <https://www.R-project.org/>, last access: 24 January 2025, 2022.

789 Rahman, M. S., Ahmed, B., and Di, L.: Landslide initiation and runout susceptibility modeling in the context of hill  
790 cutting and rapid urbanization: a combined approach of weights of evidence and spatial multi-criteria, *J.*  
791 *Mt. Sci.*, 14(10), 1919-1937, <https://doi.org/10.1007/s11629-016-4220-z>, 2017.

792 Ran, Q., Wang, J., Chen, X., Liu, L., Li, J., and Ye, S.: The relative importance of antecedent soil moisture and  
793 precipitation in flood generation in the middle and lower Yangtze River basin, *Hydrol. Earth Syst. Sci.*,  
794 26(19), 4919-4931, <https://doi.org/10.5194/hess-26-4919-2022>, 2022.

795 Rathore, S. S., and Kumar, S.: A decision tree regression-based approach for the number of software faults prediction,  
796 *ACM SIGSOFT Software Engineering Notes*, 41(1), 1-6. <https://doi.org/10.1145/2853073.2853083>, 2016.

797 Razakova, M., Kuzmin, A., Fedorov, I., Yergaliev, R., and Ainakulov, Z.: Methods of calculating landslide volume  
798 using remote sensing data, In E3S Web of Conferences (Vol. 149, p. 02009), EDP Sciences,  
799 <https://doi.org/10.1051/e3sconf/202014902009>, 2020.

800 Rosi, A., Peternel, T., Jemec-Auflič, M., Komac, M., Segoni, S., and Casagli, N.: Rainfall thresholds for rainfall-  
801 induced landslides in Slovenia, *Landslides*, 13, 1571-1577, <https://doi.org/10.1007/s10346-016-0733-3>,  
802 2016.

803 Rotaru, A., Oajdea, D., and Răileanu, P.: Analysis of the landslide movements, *Int. J. Coal Geol.*, 1(3), 70-79, Available  
804 at <https://naun.org/multimedia/NAUN/geology/ijgeo-10.pdf>, last access: 24 January 2025, 2007.

805 Saito, H., Korup, O., Uchida, T., Hayashi, S., and Oguchi, T.: Rainfall conditions, typhoon frequency, and  
806 contemporary landslide erosion in Japan, *Geology*, 42(11), 999-1002, <https://doi.org/10.1130/G35680.1>,  
807 2014.

808 Saleh, A. M. E., Arashi, M., and Kibria, B. G.: Theory of ridge regression estimation with applications, John Wiley  
809 and Sons, ISBN: 9781118644614, 2019.

810 Sato, T., Katsuki, Y., and Shuin, Y.: Evaluation of influences of forest cover change on landslides by comparing rainfall-  
811 induced landslides in Japanese artificial forests with different ages, *Sci. Rep.*, 13(1), 14258,  
812 <https://doi.org/10.1038/s41598-023-41539-x>, 2023.

813 Scheidl, C., Heiser, M., Kamper, S., Thaler, T., Klebinder, K., Nagl, F., Lechner, L., Markart, G., Rammer, W., and  
814 Seidl, R.: The influence of climate change and canopy disturbances on landslide susceptibility in headwater  
815 catchments, *Sci. Total Environ.*, 742, 140588, <https://doi.org/10.1016/j.scitotenv.2020.140588>, 2020.

816 Seger, C.: An investigation of categorical variable encoding techniques in machine learning: binary versus one-hot  
817 and feature hashing, Available at [https://www.diva-  
818 portal.org/smash/get/diva2:1259073/FULLTEXT01.pdf](https://www.diva-portal.org/smash/get/diva2:1259073/FULLTEXT01.pdf), last access: 24 January 2025, 2018.

819 Shirzadi, A., Shahabi, H., Chapi, K., Bui, D. T., Pham, B. T., Shahedi, K., and Ahmad, B. B.: A comparative study  
820 between popular statistical and machine learning methods for simulating volume of landslides, *Catena*,  
821 157, 213-226, <https://doi.org/10.1016/j.catena.2017.05.016>, 2017.

822 Singh, D., and Singh, B.: Feature wise normalization: An effective way of normalizing data, *Pattern Recognition*, 122,  
823 108307, <https://doi.org/10.1016/j.patcog.2021.108307>, 2022.

824 Smith, H. G., Neverman, A. J., Betts, H., and Spiekermann, R.: The influence of spatial patterns in rainfall on shallow  
825 landslides, *Geomorphology*, 437, 108795, <https://doi.org/10.1016/j.geomorph.2023.108795>, 2023.

826 Stoof, C. R., Vervoort, R. W., Iwema, J., Van Den Elsen, E., Ferreira, A. J. D., and Ritsema, C. J.: Hydrological  
827 response of a small catchment burned by experimental fire, *Hydrol. Earth Syst. Sci.*, 16(2), 267-285,  
828 <https://doi.org/10.5194/hess-16-267-2012>, 2012.

829 Sun, H. Y., Wong, L. N. Y., Shang, Y. Q., Shen, Y. J., and Lü, Q.: Evaluation of drainage tunnel effectiveness in  
830 landslide control, *Landslides*, 7, 445-454, <https://doi.org/10.1007/s10346-010-0210-3>, 2010.

831 Székely, G. J., Rizzo, M. L., and Bakirov, N. K.: Measuring and testing dependence by correlation of distances,  
832 <https://doi.org/10.1214/009053607000000505>, 2007.

833 Tacconi Stefanelli, C., Casagli, N., and Catani, F.: Landslide damming hazard susceptibility maps: a new GIS-based  
834 procedure for risk management, *Landslides*, 17, 1635-1648, <https://doi.org/10.1007/s10346-020-01395-6>,  
835 2020.

836 Tsai, T. L., and Chen, H. F.: Effects of degree of saturation on shallow landslides triggered by rainfall, *Environ. Earth  
837 Sci.*, 59, 1285-1295, <https://doi.org/10.1007/s12665-009-0116-3>, 2010.

838 Turner, T. R., Duke, S. D., Fransen, B. R., Reiter, M. L., Kroll, A. J., Ward, J. W., Bach, J. L., Justice, T. E., and Bilby,  
839 R. E.: Landslide densities associated with rainfall, stand age, and topography on forested landscapes,  
840 southwestern Washington, USA, *For. Ecol. Manag.*, 259(12), 2233-2247, [https://doi.org/10.1016/  
841 j.foreco.2010.01.051](https://doi.org/10.1016/j.foreco.2010.01.051), 2010.

842 Um, M. J., Yun, H., Cho, W., and Heo, J. H.: Analysis of orographic precipitation on Jeju-Island using regional  
843 frequency analysis and regression, *Water Resour. Manag.*, 24, 1461-1487, [https://doi.org/10.1007/s11269-  
844 009-9509-z](https://doi.org/10.1007/s11269-009-9509-z), 2010.

845 Van Westen, C. J.: The modelling of landslide hazards using GIS, *Surv. Geophys.*, 21(2), 241-255,  
846 <https://doi.org/10.1023/A:1006794127521>, 2000.

847 Wang, D., Hollaus, M., Schmaltz, E., Wieser, M., Reifeltshammer, D., and Pfeifer, N.: Tree stem shapes derived from  
848 TLS data as an indicator for shallow landslides, *Procedia Earth Planet. Sci.*, 16, 185-194,  
849 <https://doi.org/10.1016/j.proeps.2016.10.020>, 2016.

850 Wei, Z. L., Shang, Y. Q., Sun, H. Y., Xu, H. D., and Wang, D. F.: The effectiveness of a drainage tunnel in increasing  
851 the rainfall threshold of a deep-seated landslide, *Landslides*, 16, 1731-1744,  
852 <https://doi.org/10.1007/s10346-019-01241-4>, 2019.

853 Wieczorek, G.: Debris flows/avalanches: process, recognition, and mitigation, Volume VII, GSA, Boulder, Colorado,  
854 ISBN:0-8137-4107-6, 1987.

855 Willmott, C. J., and Matsuura, K.: Advantages of the mean absolute error (MAE) over the root mean square error  
856 (RMSE) in assessing average model performance, *Climate Res.*, 30(1), 79-82,  
857 <https://doi.org/10.3354/cr030079>, 2005.

858 Yan, L., Xu, W., Wang, H., Wang, R., Meng, Q., Yu, J., and Xie, W. C.: Drainage controls on the Donglingxing  
859 landslide (China) induced by rainfall and fluctuation in reservoir water levels, *Landslides*, 16, 1583-1593,  
860 <https://doi.org/10.1007/s10346-019-01202-x>, 2019.

861 Yoon, S. S., and Bae, D. H.: Optimal rainfall estimation by considering elevation in the Han River Basin, South Korea,  
862 *J. Appl. Meteorol. Climatol.*, 52(4), 802-818, <https://doi.org/10.1175/JAMC-D-11-0147.1>, 2013.

863 Yun, H. S., Um, M. J., Cho, W. C., and Heo, J. H.: Orographic precipitation analysis with regional frequency analysis  
864 and multiple linear regression, *Korea Water Resour. Assoc.*, 42(6), 465-480,  
865 <https://doi.org/10.3741/JKWRA.2009.42.6.465>, 2009.

866 Yune, C. Y., Jun, K. J., Kim, K. S., Kim, G. H., and Lee, S. W.: Analysis of slope hazard-triggering rainfall  
867 characteristics in Gangwon Province by database construction, *J. Korean Geotech. Soc.*, 26(10), 27-38.  
868 <https://doi.org/10.7843/kgs.2010.26.10.27>, 2010.

869 Zaruba, Q., and Mencl, V.: Landslides and their control, Elsevier, ISBN: 0444600760, 9780444600769, 2014.

870 Zhang, K., Wang, S., Bao, H., and Zhao, X.: Characteristics and influencing factors of rainfall-induced landslide and  
871 debris flow hazards in Shaanxi Province, China, *Nat. Hazards Earth Syst. Sci.*, 19(1), 93-105,  
872 <https://doi.org/10.5194/nhess-19-93-2019>, 2019.